2008

Microwave frequency doubler integrated with miniaturized planar antennas

Suzette Marie Presas
University of South Florida

Microwave Frequency Doubler Integrated with Miniaturized Planar Antennas

by

Suzette Marie Presas

A thesis submitted in partial fulfillment
of the requirements for the degree of
Master of Science in Electrical Engineering
Department of Electrical Engineering
College of Engineering
University of South Florida

Major Professor: Thomas M. Weller, Ph.D.
Andrew M. Hoff, Ph.D.
James T. Leffew, Ph.D.

Date of Approval:
May 22, 2008

Keywords: frequency doubling reflectenna, diode doubler, conversion efficiency, compact microstrip antenna, meandered antennas, tunable

To my father Pompeyo Aguilar,
for showing me among many things the concept of √.
To my mother Sonia Wiemer,
for teaching me about persistence.

To my Nina,
for giving me her love and strength;
you are the light that keeps me going.

TABLE OF CONTENTS

LIST OF TABLES

LIST OF FIGURES

Microwave Frequency Doubler Integrated with Miniaturized Planar Antennas

Suzette Marie Presas

ABSTRACT

In this thesis the development of a high efficiency harmonic re-radiator, consisting of a diode doubler and conjugate-matched receive and transmit antennas, is described. Diode-based frequency multipliers and rectifiers, coupled with antennas, are of interest for quasi-optical applications, for energy-scavenging and for sensing applications. The device studied operates by receiving an interrogating signal at a frequency of 1.3 GHz and re-radiating a signal at 2.6 GHz. The primary goal of this research was to develop a passive, miniature and effective frequency doubler integrated with planar antennas. The system is referred to as a frequency doubling reflectenna, (FDR). Prediction of accurate performance was achieved by employing precise modeling and measurement methods. The FDR can be utilized in data collection applications.

The footprint of the FDR is occupied primarily by the receive and transmit antennas. Therefore, a significant portion of the research focused on the development of compact and efficient planar antennas, which would provide for a miniature FDR. A first-generation FDR design was designed, which utilized quarter-wavelength shorted microstrip patch antennas. The choice of antennas provided a small prototype with

dimensions equal to 44 mm by 17 mm. In order to further reduce the size of the harmonic re-radiator, meandered planar antennas were investigated and optimized for efficient operation. A second-generation FDR design, which utilized meandered microstrip patch antennas, was produced and a size reduction of 75% was achieved. Both first- and second-generation harmonic re-radiator designs were designed for low input power operation and provided maximum measured conversion efficiencies of approximately 4.5% and 1.8%, with the input to the diode doubler at -14.5 and -17.5 dBm, respectively.

Re-configurable microwave devices, which dynamically operate at different frequencies, are often desirable for sensing applications. Therefore, to conclude this research, a tunable FDR was realized using a semiconductor varactor that provided the dynamic capacitance required for the tunability.

PREFACE

I am humbled by the opportunity of encountering great individuals that have believed in me throughout my life. My deep appreciation goes to all of them.

I will be eternally grateful to Professor Tom Weller for introducing me to the field of microwaves and for his guidance and insight on this work and various other matters. I especially appreciate his enthusiasm of conveying a true understanding of the subject and his exceptional dedication to the field, both of which are tremendous inspirations to me.

I am extremely thankful to Dr. James Leffew for his enlightenment on Electrical Engineering topics and for patiently editing the different portions of this thesis. I am grateful to Dr. Andrew Hoff for his suggestions during the course of this work.

Thank you, Henrry La Rosa for sharing your knowledge and time during all of our EE studies; you have shown me how to become a better engineer. Dr. Saravana P. Natarajan, you are a kind and generous character, and I am grateful for all your help, especially for your assistance with fabrication and for your practical views of life. Bojana Zivanovic, I will always cherish our memories together, our travels, and the much-needed times when you have provided your electromagnetic expertise, reason, and humor. I am indebted to Sergio Melais for providing guidance on antenna radiation pattern analysis and for always making my days at 412 just brighter. Bojana and Sergio, you are family. I am thankful to Diana Aristizabal and Sam Baylis for furthering my understanding of RF techniques and early on serving as my microwave research mentors.

The encouragement given by Alberto Rodríguez to become an electromagnetic academic is much appreciated. My sincere regards go to Ebenezer Odu for your caring nature. I appreciate assistance with nanocrystalline diamond provided by Srinath Balachandran. For their company in ENB 412, I am grateful to: Quenton Bonds, Evelyn Benabe, Tony Price, Aswin Jayaraman, Dr. Tom Ricard and Daniel Sosa Martin. For conversations that enriched my life in various ways, my regards go to: James Mcknight, Scott Skidmore and Lance Nettles. I appreciate the fabrication assistance provided by Subbu Krishnan. Special thanks go to Norma Paz for her sweet encouragement at various times.

For financial support, I am in gratitude to Raytheon Systems (Fullerton, CA), to the NSF (NIRT Project ECS-0404137), to the NSF IGERT Program (Grant DGE 0221681), and to the USF Graduate School, especially Mr. Rod Hale. Special thanks to Modelithics, Inc. for allowing me to use their lab facilities and measurement equipment.

I would have never come this far without my family's and friends' love and support. I wish to express my deep appreciation to friends that have always believed in what I can accomplish: Gail, Alex, Mario, Jessica, and Diana. For her incredible kindness and strength, I would like thank Loly Valmaña. I am grateful to my mother for encouraging me to approach life with a graceful spirit, and to my father, my scholar, for teaching me to love all knowledge for the sake of knowledge with the passion that only you could have. I would like to thank my sister Tatiana, to me the most unique person in the world; your doses of comedy and sensitivity remarkably enrich my life every day.

Finally I would like to give eternal loving thanks to Axel; I will be forever appreciative of your noble and philosophical spirit and your charisma. My infinite thanks go to you for revealing such a marvelous world of hopefulness to me.

CHAPTER 1

INTRODUCTION

Great advances have been made in microwave integrated circuit technology since the development of planar transmission lines and microwave solid-state devices. Microstrip lines have become an integral part of microwave integrated circuits due to their low-cost, small size, ease in manufacturing, ease of active and passive device integration and good repeatability and reproducibility associated with these transmission lines, [1]. In addition, since their first practical implementations in the 1970s, microstrip antennas have been one of the most commonly used radiators for integrated circuit applications. In the area of solid-state devices, research associated with semiconductor diodes has led to the development of components such as frequency multipliers. Numerous studies have concentrated on building more efficient and compact integrated microwave circuits. As a result, microstrip antennas have been integrated with other microstrip circuits to produce small designs and to maximize the efficiency of solid-state devices, which may be employed in the circuitry, [2]. Additionally, advances realized in computer-aided design and in manufacturing and processing techniques greatly assisted the development of novel integrated designs.

The research described in this thesis focused on producing a simple, low-cost, low-power and miniature diode frequency multiplier integrated with planar antennas.

Integrating antennas with other components has been accomplished in quasi-optical applications and wireless power transmission. However, the main application for the devices described in this thesis is in wireless sensors nodes.

This research concentrated on a passive harmonic re-radiator scheme. The re-radiator receives an interrogation signal at a fundamental frequency and re-radiates a signal back to a transceiver at the second harmonic. Harmonic re-radiation can alleviate the clutter radiation that occurs at the frequency of the incident radiation in a radar transceiver system. Since sensor nodes may be located in remote areas and subjected to harsh conditions, a robust, compact, efficient and reliable device was desired. Consequently, the design consists of a Schottky beamlead diode, which is used as the frequency multiplier, and compact microstrip antennas, which receive and transmit the signal. Schottky beamlead diodes have been proven to perform well at microwave frequencies and microstrip antennas are often utilized in low-power transmitting and receiving applications, [2].

1.1 Frequency Multiplication

Frequency multipliers have been used primarily as signal generators to produce high-frequency local oscillator signals. Frequency multiplication is possible due to the inherent nonlinearities present in certain electronic components. When these nonlinear devices are excited with a sinusoidal waveform at one particular frequency, the resulting response is a distorted waveform composed of harmonics. The operating principle of harmonic generation for a device employing nonlinear capacitance is presented in Figure 1.1.

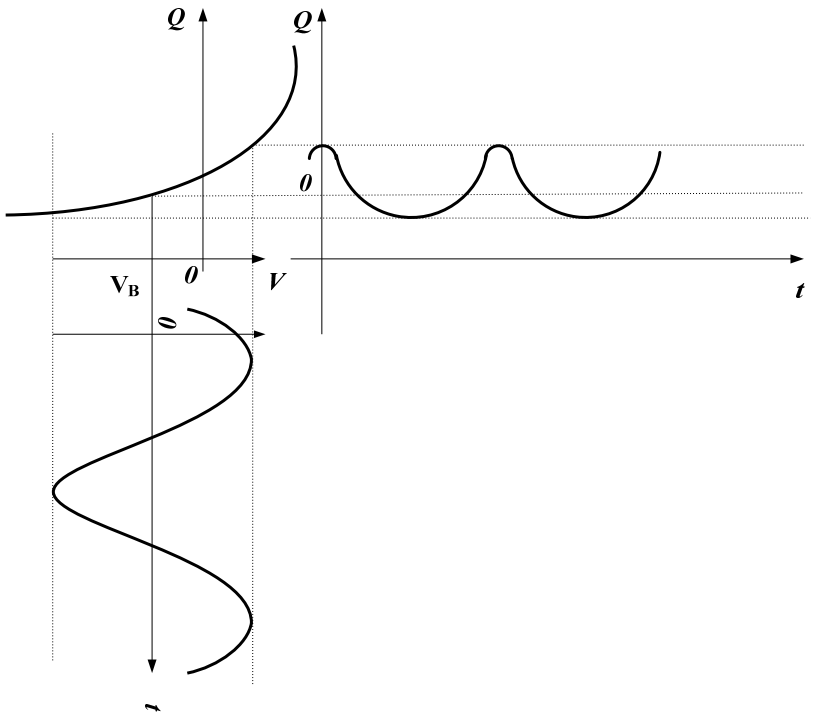

Figure 1.1: Operating Principle of a Frequency Multiplier Using Nonlinear Capacitance, [3]

A nonlinear charge-voltage characteristic can be expressed as a power series about an operating point, V_B, which denotes the bias voltage, [3]. The power series expression for the bias voltage is given by:

$$Q(V_B + \Delta V) = b_o + b_1 \Delta V + b_2 \Delta V^2 + b_3 \Delta V^3 + \ldots . \tag{1.1}$$

The input voltage applied to the device is given by:

$$\Delta V = V_d \cos(w_g t) . \tag{1.2}$$

Substitution of equation (1.2) into equation (1.1) yields:

$$Q(t) = Q_o + Q_1 \cos(w_g t) + Q_2 \cos(2w_g t) + Q_3 \cos(3w_g t) + \ldots, \tag{1.3}$$

which is an expression that highlights the input signal harmonics.

In passive frequency multiplier designs, a device with a nonlinear current-voltage (varistor) or capacitance-voltage (varactor) characteristic may be utilized. In fact, real devices present both nonlinearities. Devices utilized in a frequency conversion process must have strong nonlinearities and repeatable electrical properties. As a result, semiconductor *p-n* junction diodes and metal-semiconductor junction diodes, which are usually called Schottky barrier or Schottky diodes, are often utilized. Schottky barrier diodes are usually preferred since they are majority carrier devices and metal-semiconductor junctions can be fabricated in a more precise and repeatable manner, [3]. Multipliers based on nonlinear transmission lines have also been reported, [4-6].

1.2 Frequency Multipliers and Detectors Integrated with Antennas

Diode-based frequency multipliers and rectifiers, coupled with antennas, have been of interest in quasi-optical applications, in wireless power transmission and in wireless sensors applications. Numerous works have been presented on frequency multipliers integrated with antennas for quasi-optical receiver applications and power combining architectures at millimeter and sub-millimeter wave frequencies, [7-11]. One of these architectures is illustrated in Figure 1.2.

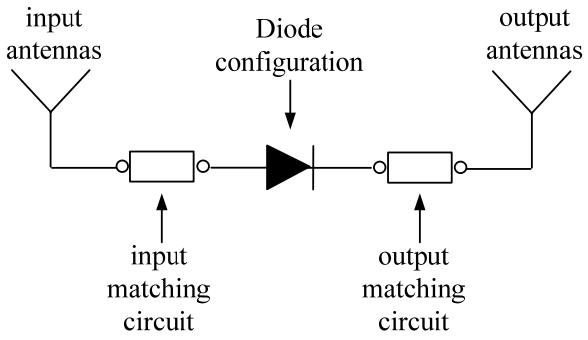

Figure 1.2: Quasi-Optical Frequency Diode Doubler Scheme, [9]

Since the output power of solid-state devices decreases as the frequency of operation increases, quasi-optical techniques are used to combine the power of several solid-state devices. Moreover, diodes coupled with antennas have also been utilized in wireless power transmission applications, [12-14]. For instance, a high-sensitivity CMOS rectifier, which can recharge a secondary battery for sensor network systems and be utilized in a low-power wireless transmission system has been reported, [14]. Similarly, rectennas (rectifying antennas) have been used to receive power where no physical connections are possible.

Several types of rectennas have been presented where the main parameter of interest is the RF-to-dc conversion efficiency. A dual-frequency rectenna operating at both 2.45 GHz and 5.8 GHz has been successfully designed. The design utilized a printed dual-frequency dipole antenna. The antenna was integrated with low-pass and bandstop filters to block higher order harmonics generated from a GaAs Schottky barrier diode, [12]. The diode is directly connected to the filters and the conversion efficiency maximized by matching the diode's input impedance to the filters impedance. Chang et al., also developed a similar design where the rectenna circuitry consists primarily of a high-gain antenna and a Schottky diode. These components are integrated with a band-

reject filter, a dc filter and a resistive load. A basic block diagram of this device is presented in Figure 1.3, [13].

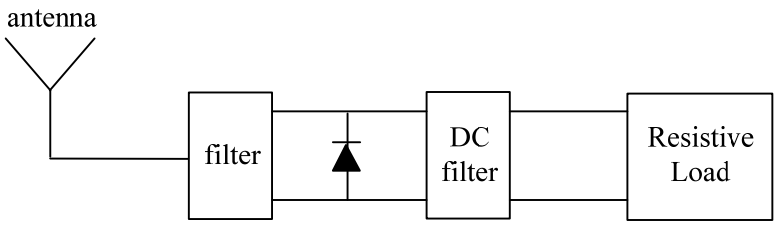

Figure 1.3: Rectenna Block Diagram, [13]

In both of these rectenna designs, RF-to-dc conversion efficiencies of approximately 80% were achieved for received powers on the rectenna's antenna of 15.5 – 20 dBm.

In the context of wireless sensors, Ketterl et al. introduced a reflectenna design that consists of a receive antenna, a device, such as a switch, that modulates a received continuous wave and a transmit antenna that redirects the modulated signal back to the transmission source, [15]. This design was intended for a low-power application. Additionally, a miniature harmonic radar transceiver design, which utilizes a short length of wire to form the antenna and a beamlead Schottky diode as the doubling element, has been reported and utilized for insect tracking, [16]. The authors of this study employed a harmonic radar receiver that was tuned to the second harmonic of the transmitter. This configuration eliminates the conventional radar scatter. Riley et al., also presented transponders, which consisted of a similar design, for insect tracking purposes as well, [17].

Other types of wireless sensor circuits include RF identification (RFID) transponders and surface acoustic wave (SAW) sensors. These sensors can be classified as active devices, which are powered by a battery and as passive transponder devices,

which are not battery powered. One of the first applications of SAW sensors was for temperature sensing, [18]. A one-port reflective SAW device was connected to an antenna and interrogated by an RF signal, [18-21]. The SAW device usually consists of a piezoelectric substrate with metallic structures, which are interdigital transducers on the polished surface. A SAW is stimulated at the surface due to an electric signal at the interdigital transducer. Temperature, mechanical stress or bending can cause a delay change or frequency shift of the retransmitted signal sent by the SAW device to a transceiver. SAW sensors for humidity, pressure, position, acceleration, wear, magnetic field and electric current have been developed, [18].

In a similar fashion, RFID tags also receive an interrogator signal from a unit designated as the reader. These transponders are utilized in areas such as manufacturing, retailing, transport and security, [22]. The RFID tags consist of an antenna and of an integrated circuit (IC) chip, which is capable of storing information. Data transfer occurs between the reader and the tag through antennas linked to both ends. Passive RFID tags, which are the most widely used, are powered by restoring the electromagnetic energy emitted from the reader. The transponders communicate with the reader by modulating the RF energy received and by creating a backscatter signal. A study of modulated backscatter RFID transponders can be explored further in [23]. A complete analysis for the estimation of the backscattered radiated field of a UHF RFID tag is presented in [24]. Different types of antennas have been proposed for RFID tags such as dipole antennas, [25], planar inverted-F antennas, [26-27], and printed patch antennas, [28]. The detector diode most frequently used in the IC of the RFID tag is the Schottky barrier diode.

Several authors have demonstrated that higher conversion efficiencies can be obtained by using active frequency multipliers integrated with antennas, [29-30]. Itoh et al. have extensively explored the concept of active integrated antennas with frequency multipliers, [31-33]. Although higher conversion efficiencies are obtainable, some active frequency multipliers involve complex circuitry, due to biasing considerations, which may lead to higher manufacturing costs.

1.3 Frequency Doubling Reflectenna

The research presented in this thesis centers on the design of a diode frequency doubler integrated with antennas. The device is referred to as a Frequency Doubling Reflectenna, (FDR). This device was created primarily for sensing applications. The FDR receives a signal at a fundamental frequency and re-radiates the signal back to a transceiver at the second harmonic. It was of interest to obtain a design with minimum conversion loss for a low-power input (-30 dBm), as well as sufficient sensitivity for the data collection application. The energy of the interrogator signal was used effectively to power the solid-state device employed, which produced a simple passive design, [34]. Figure 1.4 demonstrates the FDR concept.

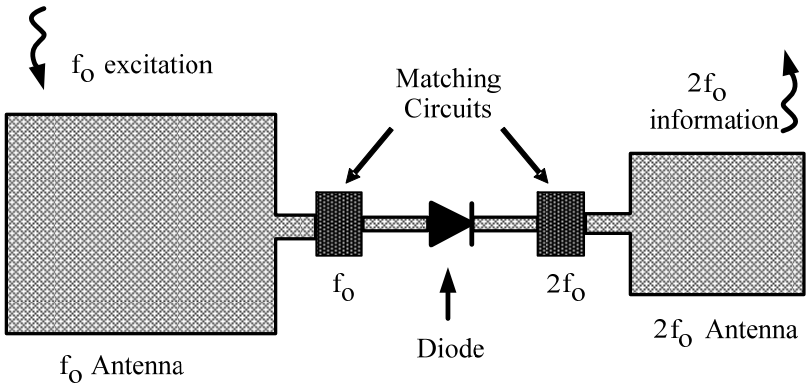

Figure 1.4: Frequency Doubling Reflectenna Concept, [34]

Efficiency and compactness were primarily achieved by conjugate matching the input impedances of the receive and transmit antennas to the diode terminals. Moreover, reduction in size was attained by utilizing electrically small patch antennas. Proper simulation methods and modeling techniques proved to be essential for the accurate prediction of device performance. It was also of importance to demonstrate the concept of a tunable FDR. In the tunable device, maximum re-radiation occurs at the first harmonic in an on-state, and no re-radiation occurs in an off-state. Tunability was provided by a semiconductor varactor, which is a variable reactance device. Features of the device such as its miniature size, frequency selectivity and reliable operation, make the FDR very useful in sensing applications. Although this thesis refers to a FDR operating at 1.3 GHz – 2.6 GHz, the design can be considered a proof-of-concept and scaled to other operating frequencies.

1.4 Overview and Contributions of the Research

The primary goals of this research were

- Accurately predict the behavior of a frequency doubler integrated with receive and transmit antennas,
- Design the FDR in a manner that would maximize conversion efficiency,
- Produce a simple and compact integrated device.

Chapter 2 presents the work performed in designing, fabricating, and testing a 1.3 GHz – 2.6 GHz frequency doubling reflectenna. Chapter 2 also addresses topics such as the Schottky diode model used in the doubler, the circuit schematic modeling of the FDR, the quarter-wavelength shorted patch antennas utilized in the first-generation design and the measurement test-bench employed. It is noteworthy to mention that a conversion efficiency of 1% was obtained for a low input power of -30 dBm.

The following two chapters describe the progression toward a miniature and tunable FDR design. Chapter 3 provides a study of current electrically small antenna technology with an emphasis on meandered antennas. In addition, Chapter 3 also presents a description of the design of the miniature meandered patch antennas utilized in a second-generation 1.3 GHz – 2.6 GHz FDR design. The miniature meandered patch antennas represent approximately an 85% reduction in size from the patch antennas utilized in the first-generation design. In Chapter 4, a miniature and tunable FDR is presented. A summary of the findings of this research as well as suggestions for future work are presented in Chapter 5.

CHAPTER 2

FREQUENCY DOUBLING REFLECTENNA
1.3 GHz – 2.6 GHZ

2.1 Introduction

Frequency multipliers based on diodes offer low-cost, high reliability and can be easily integrated with other semiconductor components by utilizing planar technology. Diode-based frequency multipliers and rectifiers, coupled with antennas, are of interest in quasi-optical applications, energy-scavenging, and sensing applications, [7-33]. In addition to obtaining a compact device, an integrated diode frequency multiplier/antenna module alleviates the requirement to separately design for the two components and then combine them under certain impedance constraints.

In this chapter, a frequency doubling reflectenna, (FDR), which receives a 1.3 GHz interrogation signal and re-radiates a 2.6 GHz signal, is described. The topology of the FDR is presented in Figure 2.1.

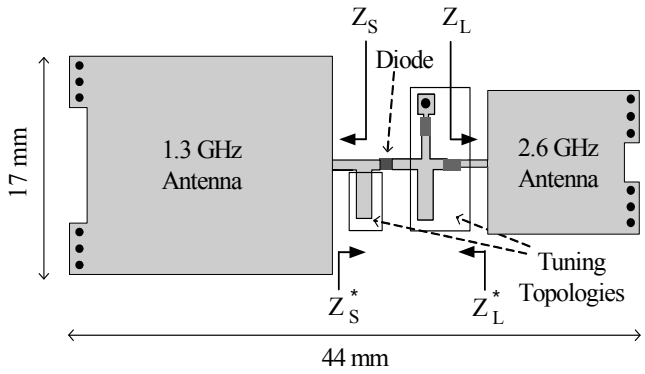

Figure 2.1: Layout of a Frequency Doubling Reflectenna with Conjugate-Matched Impedances

The FDR is intended for sensing applications. Therefore, to enhance the ability of the interrogating transceiver to detect a very low-power return signal, the FDR utilizes frequency discrimination. A GaAs Schottky diode was used as the doubling element. The GaAs Schottky diode is a proven reliable device for generating power at microwave frequencies compared to other semiconductor *p-n* junction diodes. The conversion loss of a diode frequency multiplier is minimized when the source impedance is very close to the complex conjugate of the input impedance of the diode and likewise with the load impedance, [3]. Both the receive and transmit antenna were designed to be conjugate-matched to the diode multiplier in order to minimize the footprint and maximize the conversion efficiency. As illustrated in Figure 2.1, Z_S and Z_L are the input impedances of the receive and transmit antennas, respectively. The input and output impedances of the diode circuit are presented as the complex conjugates of Z_s and Z_L. Integrating antennas with other components has been investigated in a similar fashion in quasi-optical receiver applications, [9].

Utilizing this method of component integration provided a doubler conversion efficiency of 1% at a -30 dBm input power level. Although DC bias could improve

conversion efficiency, it was not applied in the harmonic re-radiator in order to maintain a simple design. Quarter-wavelength, shorted microstrip patch antennas were used to reduce the overall size of the FDR, [2]. In this design, the antennas provide a natural DC return for the doubler. In addition, they also inherently provide the proper harmonic impedance at 2.6 GHz at the input and at 1.3 GHz at the output. Due to the conjugate-match approach, the resulting design was very narrowband and the desired sensitivity was achieved. Inclusion of the correct harmonic terminations in circuit simulations for the FDR yielded comparisons between measured and predicted conversion efficiency within tenths of a dB.

2.2 Circuit Overview

A GaAs Schottky diode was utilized in the harmonic re-radiator to obtain frequency multiplication. The GaAs Schottky diode is a nonlinear device, which accepts the signal received by the input antenna of the FDR and produces the required harmonic. Tuning circuits were used to provide optimum source and load impedances to the Schottky diode at the input and output frequency. The output antenna of the FDR re-radiates the second order harmonic of the received signal.

In order to predict the performance of the harmonic re-radiator, simulations were performed using Agilent's Advanced Design System (ADS) CAD software. The main FDR design parameter of interest was the doubler conversion efficiency η_η, which is given by

$$\eta_n = \frac{P_{out}}{P_{in}}. \tag{2.1}$$

P_{in} is the input power to the diode multiplier, at 1.3 GHz, and P_{out} is its output power, at 2.6 GHz. Semiconductor diodes are lossy passive devices. As a result, the conversion efficiency of a diode frequency multiplier is less than unity.

2.2.1 Schottky Diode Modeling

A Schottky-barrier diode is a semiconductor device that exhibits nonlinear properties due to its metal-semiconductor contact. An electrostatic barrier arises due to unequal work functions between the metal, which forms the anode and the semiconductor, which forms the cathode. Conduction is controlled by thermionic emission of majority carriers across the barrier. The electrical characteristics of a Schottky diode are mainly determined by the metal and semiconductor contacting surfaces. High-frequency operation is optimized when the diode possesses low series resistance, low junction capacitance, high carrier mobility and high carrier saturation velocity, [3].

The nonlinear model for the HSCH-9161 beamlead diode used in the doubler is presented in Figure 2.2.

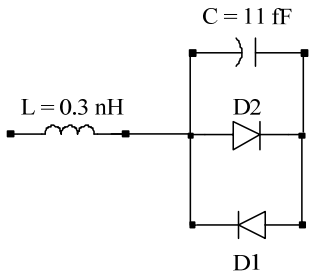

Figure 2.2: Circuit Model for the HSCH-9161
Zero-Bias Beamlead Detector Diode

The model consists of parasitic elements and an anti-parallel diode pair. The diode designated D1 represents the characteristic under forward bias of the HSCH-9161 and D2 (in the forward direction) gives the V-I curve under reverse bias of the HSCH-9161. The anti-parallel diode pair is utilized due to the high leakage of the diode under reverse bias. The *p-n* junction diode model parameters are presented in Table 2.1.

Table 2.1: *P-N* Junction Diode Model Parameters

Name	**Description**	**Unit**
I_S	Saturation current	A
R_s	Ohmic resistance	Ω
N	Emission coefficient	-
C_{j0}	Zero-bias junction capacitance	pF
V_j	Junction potential	V
M	Grading coefficient	-
XTI	Saturation-current temperature exponent	-
E_G	Energy gap	eV
B_V	Reverse break down voltage	V
I_{BV}	Current at reverse break down voltage	A

The ADS default *p-n* junction diode model parameters are presented in Table 2.2. Also shown in Table 2.2 are the SPICE model parameters that were obtained from the Agilent HSCH-9161 zero-bias beamlead detector diode data sheet. These parameters were used in order to convert the ADS basic *p-n* junction diode model. These SPICE model parameters were initially utilized in the computer-aided simulations. However, the ideality factor, (*N)*, and zero-bias junction capacitance, (Cj_o), parameters were optimized in the zero-bias region. Direct current I-V measurements, in the forward and reverse bias regions, were performed using a Keithley 4200 Semiconductor Characterization System. The characterization was accomplished by employing ground-signal-ground probing on a biased diode, which was mounted on a test fixture. After comparing measured and simulated I-V data, the ideality factor and zero-bias junction capacitance obtained were $N = 1.35$ and $Cj_o = 0.035$ pF for D1 and $N = 56$ and $Cj_o = 0.035$ pF for D2. An ideality factor that is not equal to 1 usually indicates tunneling of electrons through the electrostatic barrier between the metal and the semiconductor of the Schottky diode. The HSCH-9161 device model parameters presented include the optimized N and Cj_o values. Throughout the research, these last set of parameters were utilized for the computer-aided simulations of circuits that involved the HSCH-9161 beamlead detector diode.

Table 2.2: HSCH-9161 Beamlead Diode Parameters

Name	P-N Junction Diode Model Default	HSCH-9161 SPICE Model Parameters		HSCH-9161 Device Model Parameters	
		D1	D2	D1	D2
I_s	10^{-14}	12×10^{-6}	84×10^{-6}	12×10^{-6}	84×10^{-6}
R_s	0.0	50	10	50	10
N	1.0	1.2	40	1.35	56
C_{j0}	0.0	0.030	0.030	0.035	0.035
V_j	1.0	0.26	0.26	0.26	0.26
M	0.5	0.5	0.5	0.5	0.5
XTI	3.0	2	2	2	2
E_G	1.11	1.42	1.42	1.42	1.42
B_V	∞	10	10	10	10
I_{BV}	0.001	10^{-12}	10^{-12}	10^{-12}	1

Figures 2.3 and 2.4 illustrate good agreement, between the diode model and the measured responses, for the two diode samples in both the forward and reverse bias region near zero-bias.

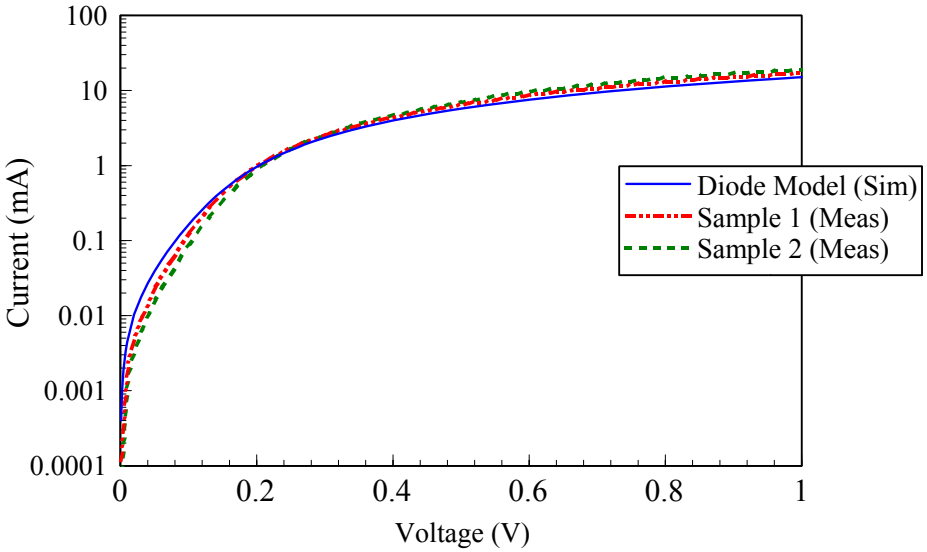

Figure 2.3: Comparison of Measured and Modeled Current versus Bias Voltage of the Schottky Diode in the Forward Bias Region

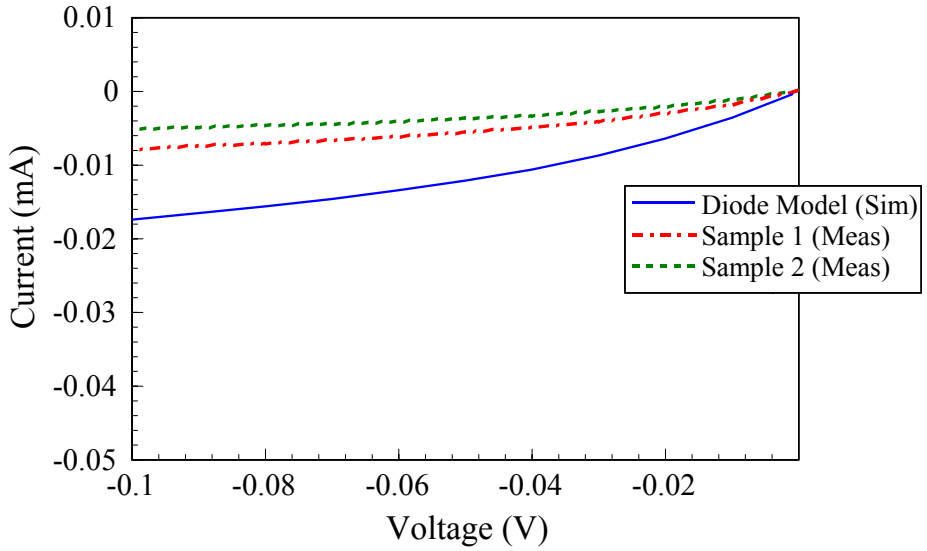

Figure 2.4: Comparison of Measured and Modeled Current versus Bias Voltage of the Schottky Diode in the Reverse Bias Region

2.2.2 Circuit Modeling of the Frequency Doubling Reflectenna

The Schottky diode is a nonlinear device, which generates the harmonics necessary for service as a frequency multiplier. Therefore, the effect of accounting for

harmonic terminations in the computer-aided analysis was studied, [3]. Figure 2.5 presents the equivalent circuit model for an FDR antenna, which can represent either the receiving or transmitting antenna.

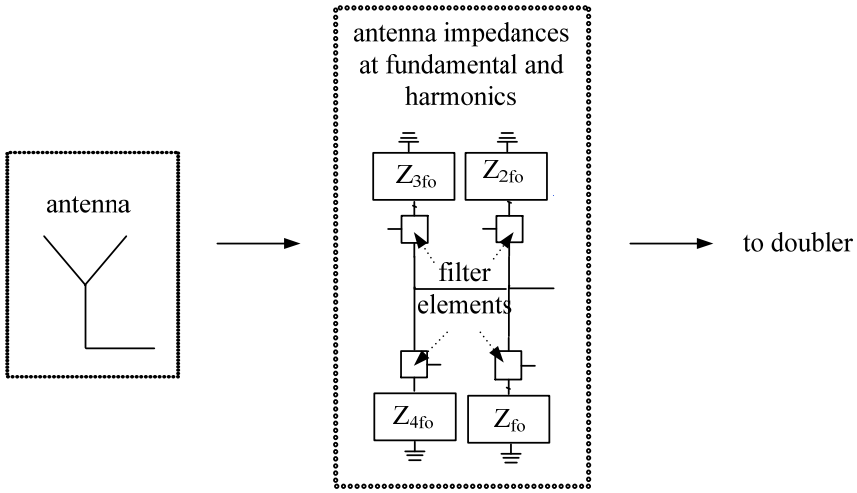

Figure 2.5: Equivalent Circuit Model of a Single FDR Antenna for Computer-Aided Analysis

In the design, produced during this research, the source and the load of the entire FDR circuit schematic are represented by the 1.3 GHz and 2.6 GHz antenna, respectively. The values of the impedances at the fundamental and harmonic frequencies were extracted from numerical electromagnetic simulations. Blocks that represented these antenna impedances at the frequencies of interest were added at the load and at the source of the diode doubler. To insure accurate simulation, data files were created and used as 'filter elements'. These 'filter elements' ensured that the proper source/load termination was presented to the doubler circuit at a given harmonic frequency. The equivalent circuit model for the diode and the input and output tuning circuits, without the antennas, are presented in Figure 2.6.

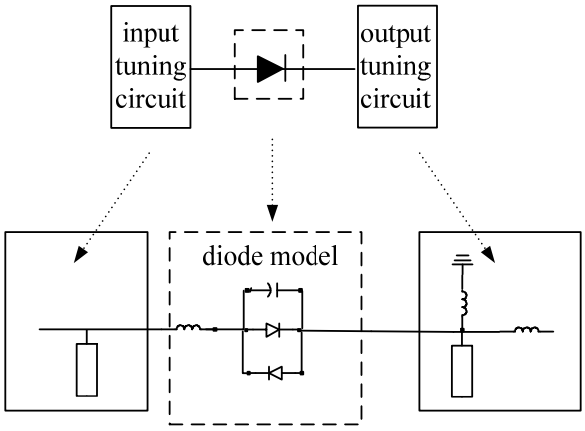

Figure 2.6: Equivalent Circuit Model of the Diode and the Input and Output Tuning Circuits of the FDR for Computer-Aided Analysis

Figure 2.7 presents the overall equivalent circuit model for the FDR.

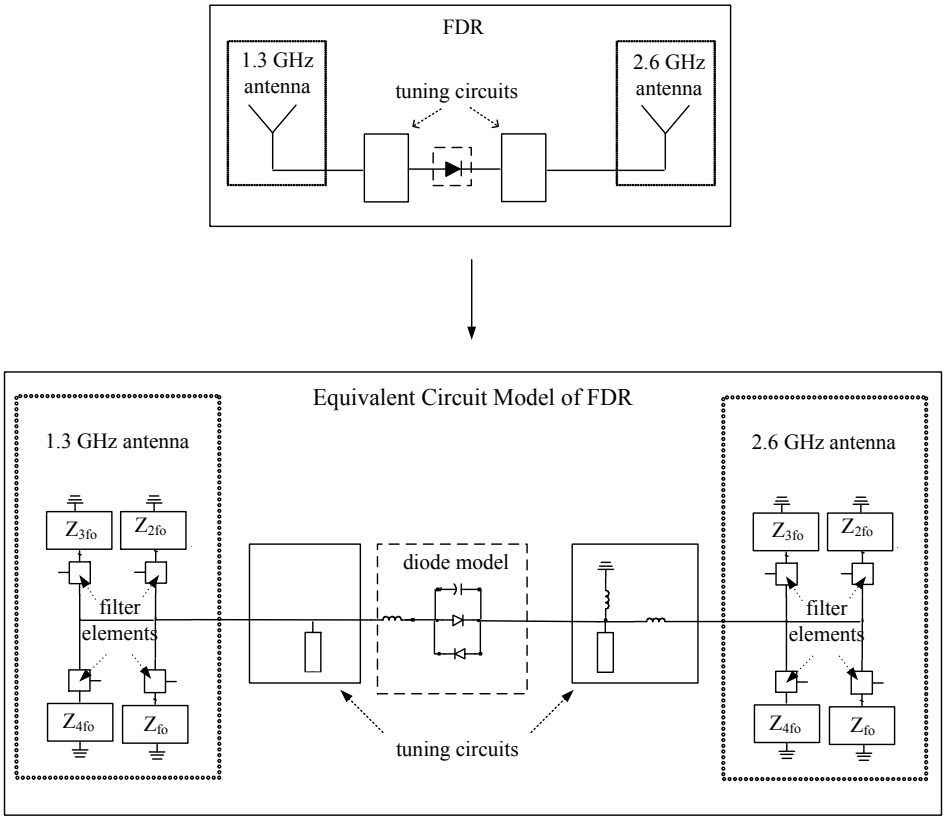

Figure 2.7: Overall Equivalent Circuit Model of Frequency Doubling Reflectenna for Computer-Aided Analysis

In order to determine the number of harmonic impedances, (*n*), to be considered in the circuit simulations, an analysis was performed to discern differences in performance between the *n* and the *n - 1* order harmonics. Figure 2.8 presents comparisons of the conversion gain of the diode doubler for several combinations of fundamental and harmonic impedances.

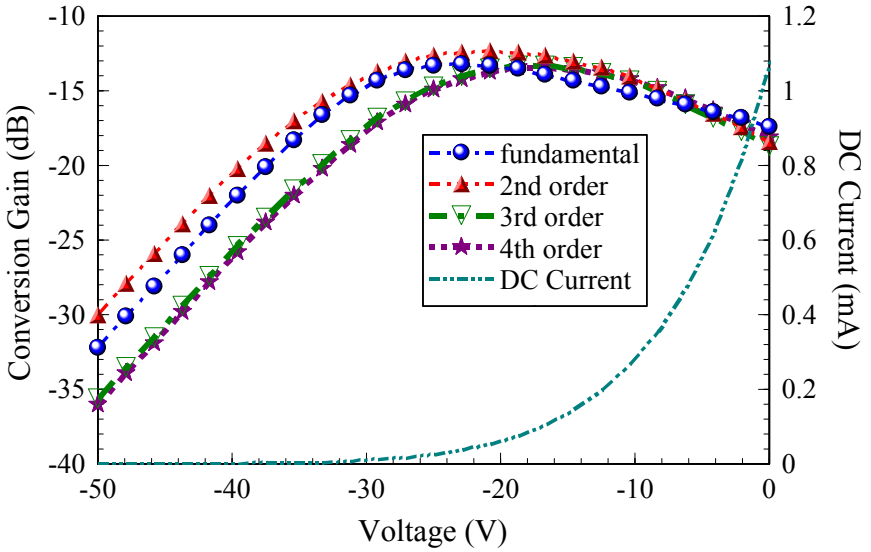

Figure 2.8: Simulated Conversion Gain and DC Current for the Diode Doubler

The difference in predicted conversion loss when considering only the 2nd order harmonic compared to including the 3rd order harmonic was ~5 dB at -30 dBm power input. However, the difference in the conversion loss between the 3rd order and 4th order harmonics was almost null. Therefore, only harmonic impedances up to the 4th order harmonic were considered. The expected conversion loss to the FDR, at an input power level of -30 dBm, was approximately 20 dB. This conversion loss was chosen as a benchmark for the remaining design considerations.

Another important observation was the predicted maximum conversion gain, which was -13.7 dB. The maximum conversion gain was obtained at the onset of the diode's DC conduction at an input power of -15.8 dBm, [35]. This is also illustrated in Figure 2.8. This behavior agrees with the fact that the region of the diode's I-V curve with the most nonlinearity occurs at the knee-voltage. This region of maximum nonlinearity serves to optimize the conversion efficiency. At higher power levels, the conversion of RF-to-DC power reduces the multiplier efficiency.

Ideally, no matching circuits are desired in order to minimize the doubler conversion loss. However, the diode frequency doubler has increased sensitivity to variations in the source and load impedance, [35]. Therefore, additional network elements were added to the basic circuit topology for fine-tuning the conjugate-match between the doubler's impedance and the antennas' impedance. A useful consequence of using quarter-wavelength shorted patch antennas, (Ref. Section 2.3), was that the input of the 1.3 GHz antenna appears as a short-circuit at 2.6 GHz, which provided the desired 2^{nd} harmonic termination. The open-circuited stub on the input side of the network was only used to fine-tune the conjugate-match. At the output, the matching topology consisted of one series 4.3 nH inductor, one shunt 2.2 nH inductor and a shunt open-circuited stub. With these tuning elements, the input and output impedance of the doubler were $(40 - j278)\ \Omega$ and $(44.7 + j369)\ \Omega$, respectively.

2.3 Quarter-Wavelength Shorted Patch Antennas

2.3.1 Design

The antennas were designed to be approximately quarter-wavelength shorted patch antennas. The ideal conjugate matching was to be performed without matching circuits in order to minimize losses. Thus, the radiation resistance of the antennas was initially set to a few ohms to match the impedance of the doubler. To validate antenna simulations, preliminary test structures, consisting of the two antennas and short and open calibration standards, were fabricated on an Arlon substrate of thickness 20 mils and a ε_r of 4.5. A circuit prototyping milling machine was used and grounding vias were filled with conductive epoxy. Figure 2.9 illustrates the board utilized to test these antennas.

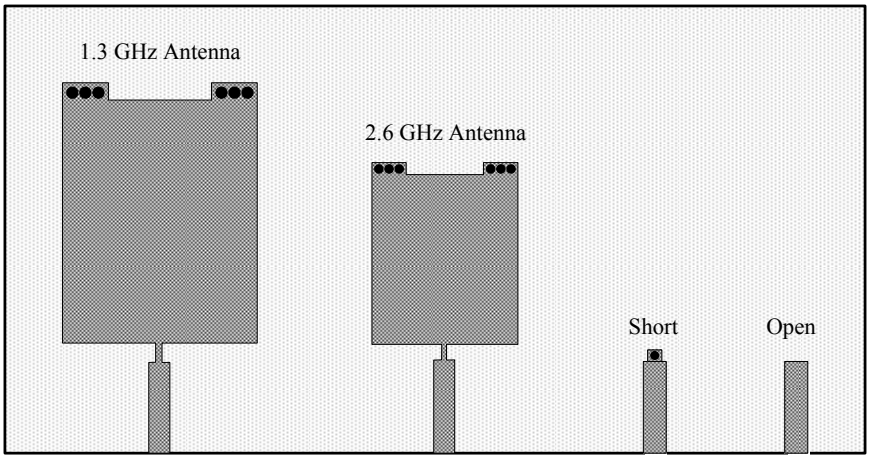

Figure 2.9: Antenna Test Board

A 3.5 mm coaxial calibration was performed, which set the reference plane at the edge of the board for measurements. Measurements of the calibration standards were used to develop a model for the PCB edge-mount connector and the feedline leading up to the reference plane, which was located approximately 1 mm from the antenna input. After the open-circuit standard was modeled it was compared with the measurements for

the short-circuit standard. The comparison indicated the need to add 1-2 Ω resistors at the via locations in order to emulate the short-circuit response. The via resistance, which was also present in the shorted patch antenna circuits, effected the antennas' return loss. Instead of being in the expected 0.5 dB range, at the frequencies of interest, the return loss was of order of 10 dB. This effect is displayed in Figure 2.10.

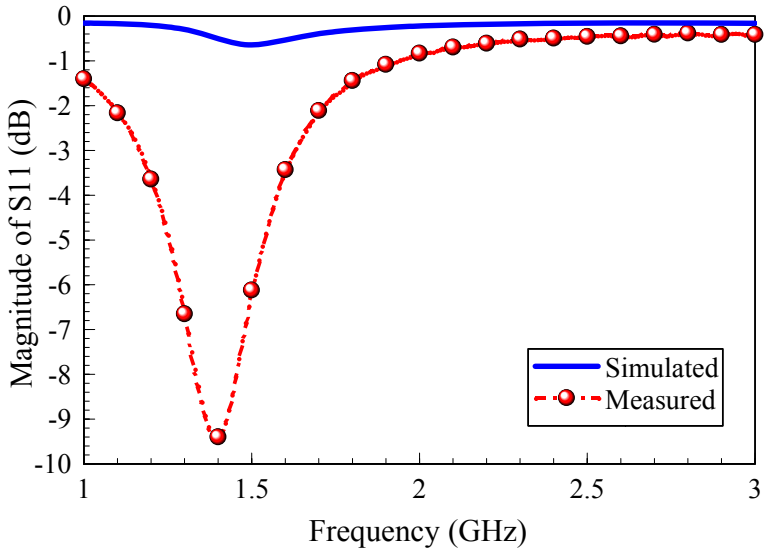

Figure 2.10: Comparison of Measured and Simulated S11 of the Preliminary 1.3 GHz Antenna Fabricated on an Arlon Substrate

The antenna efficiency depends on the radiation efficiency in accordance with

$$e = \frac{R_r}{R_r + R_L}, \tag{2.2}$$

where R_r and R_L are the radiation resistance and the loss resistance. The loss resistance, after transformation from the via location to the antenna input, increased by at least an order of magnitude with respect to the radiation resistance and dramatically reduced the antenna efficiency. This shortcoming revealed an interesting characteristic of the quarter-

wavelength antenna. The quarter-wavelength antenna performance is highly sensitive to its shorting via resistance.

A second harmonic re-radiator was designed, which accounted for this constraint. As mentioned previously, tuning circuits at the input and output of the diode frequency doubler resulted in a real impedance on the order of 40 Ω, which provided an increase in the radiation resistance of the antennas. To conjugate-match to the diode doubler, the values of width and length of each of the antennas were varied. The dimensional variations were used to change the real and imaginary values of the input impedance. The ratio of width to length can be related to the ratio of $\mathrm{Im}\{Z_{IN}\}$ to $\mathrm{Re}\{Z_{IN}\}$. An iterative optimization process was applied to the ratio in order to obtain the desired input impedance for the antenna. Figure 2.11 presents the simulated input impedance investigations for the antennas.

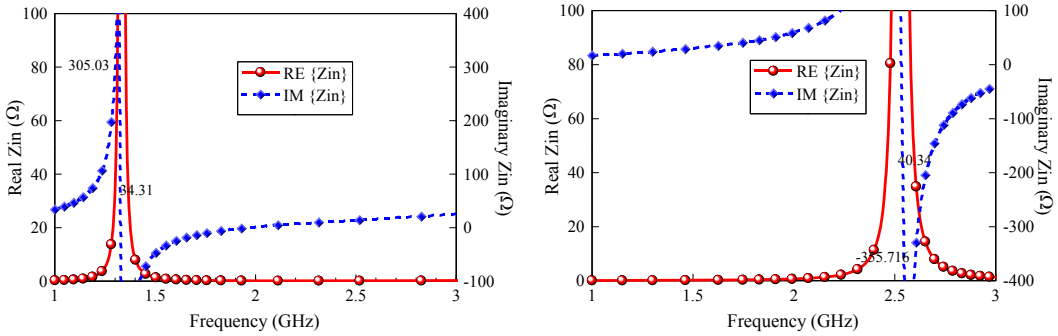

Figure 2.11: Simulated Input Impedance:
1.3 GHz Antenna (left) and
2.6 GHz Antenna (right)

The resulting 1.3 GHz antenna measured 28 mm x 21.2 mm and the 2.6 GHz antenna measured 11.25 mm x 11 mm.

Electromagnetic simulations revealed that the overall loss resistance was reduced by shorting the antenna at each side with sets of three parallel vias. To further minimize this resistance, the vias were soldered to ground using copper wires instead of silver epoxy. The measured resistance in the vias was of the order of 0.1 Ω. The board substrate was also changed to 60 mil Taconic with an ε_r of 6.15. Prior measurements of this material revealed it possessed a consistent ε_r at the desired frequencies. Figures 2.12 and 2.13 present a comparison between the measured and simulated S11 data referenced to 50 Ω for both antennas. The expected S11 data was obtained by assuming an infinite ground plane. The assumption was justified since the excitation ports available in the simulator yielded more accurate return loss values when compared to values obtained using excitation ports defined for a finite ground plane.

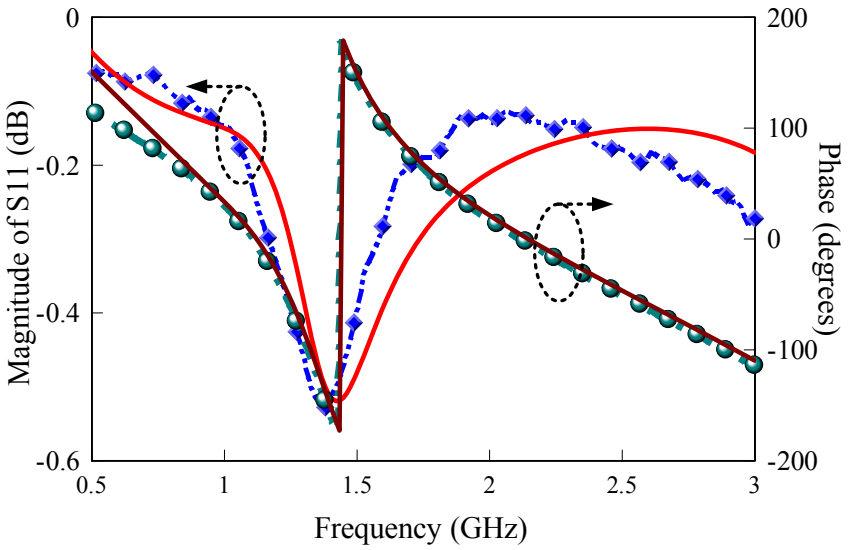

Figure 2.12: Comparison of Measured and Simulated S11 of the 1.3 GHz Antenna. Solid lines represent the simulated S11

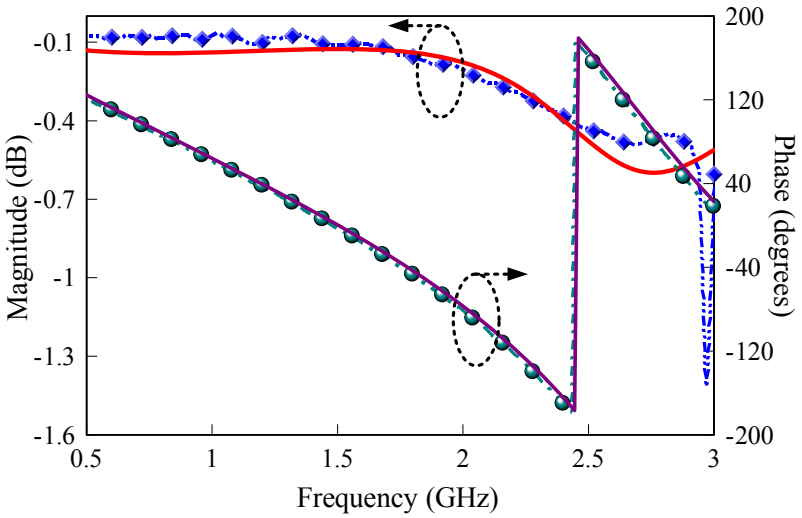

Figure 2.13: Comparison of Measured and Simulated S11 of the 2.6 GHz Antenna. Solid lines represent the simulated S11

2.3.2 Simulated and Measured Radiation Patterns

A theoretical overview of antenna radiation patterns is presented in Section 3.2. The coordinate system utilized for electromagnetic simulations of the antenna is illustrated in Figure 2.14.

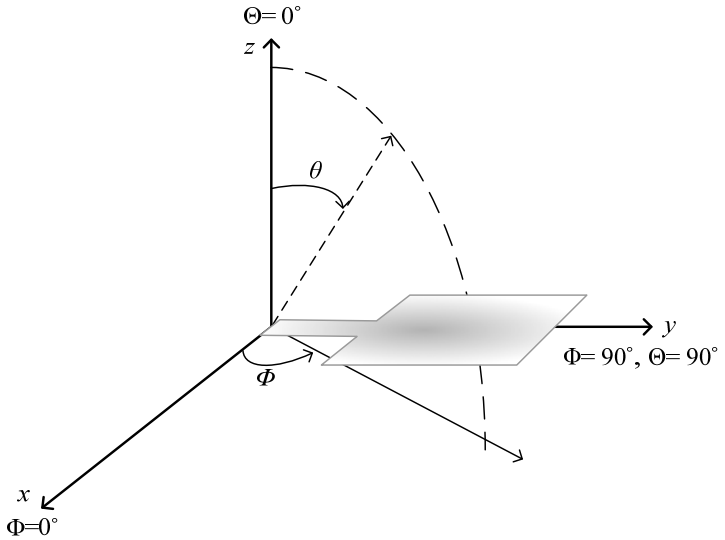

Figure 2.14: Coordinate System Used for Antenna Simulation

The radiation pattern of a patch antenna operating in the TM_{10} mode is in the broadside direction, [36]. This direction would correspond to the $\theta = 0^{\circ}$ axis for the quarter-wavelength shorted patch antennas. The shorted patch antennas were excited by a microstrip feedline, which was parallel to the direction at which the resonance occurs. Thus, they are mostly linearly polarized in the direction parallel to the microstrip feedline, which corresponds to $\Phi = 90^{\circ}$.

In a typical patch antenna, there may be a resonance that occurs at a higher frequency along the width of the antenna, which is due to higher order modes. However, at the operating frequencies of 1.3 GHz and 2.6 GHz, higher order modes are not present for these quarter-wavelength shorted patch antennas. Cross-polarization occurs since more current flows along the width of the quarter-wavelength antenna. The increased current flow does not occur in the half-wave antenna since the width to length ratio is lower. Nevertheless, the dominant polarization is along the length of the antenna.

The antenna feedline is parallel to the E-plane and perpendicular to the H-plane. The electromagnetic simulator utilized the coordinates θ and Φ to express the location of the observation point. Φ was kept fixed at 90° for E-plane simulated patterns and θ was swept 360°. Φ was kept fixed at 0° for H-plane simulated patterns and θ was swept 360°.

Simulations were initially performed by considering the ground plane of the antenna to be infinite and radiation patterns revealed no back-side radiation. Practically, compact antennas such as the quarter-wavelength shorted patch antennas studied are designed to sit on a finite ground plane. Therefore, antenna simulations were performed using a finite ground plane. The resulting radiation patterns displayed considerable back-side radiation. When the size of the ground plane was greater than the patch antenna

dimensions by approximately six times the substrate thickness, *h*, all around the edges of the patch, the results were similar to having an infinite ground plane, [36]. The size of the ground plane from the edge of the patch for both antennas is 7 mm which is less than 6*h*. Therefore, back lobes are expected in radiation patterns of these antennas.

Radiation pattern measurements were performed by placing the quarter-wavelength shorted patch antenna inside an anechoic chamber. The test antenna acted as the receive antenna. A 1.3 GHz custom dual-patch array was used as the transmit antenna and remained stationary. The receive antenna was rotated along a specified axis through 360˚. A commercial Yagi tube antenna was used as the receive antenna for the 2.6 GHz quarter-wavelength shorted patch. Rotational axes are illustrated in Figure 2.15.

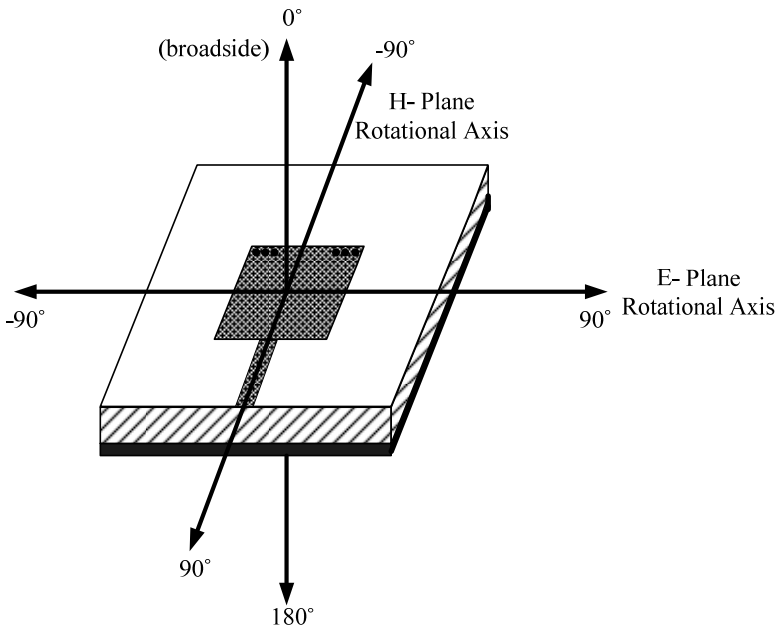

Figure 2.15: Axis Definition for Antenna Measurements

In a fashion similar to the simulations, measurements were obtained by keeping the Φ coordinate constant while sweeping the θ coordinate. The θ = 0˚ angle was defined as the

orientation where the receive and transmit antenna faces were aligned with each other. A rotation was performed about the axis perpendicular to the feedline for E-plane measurements. In contrast, H-plane measurements were obtained by rotating about the axis parallel to the feedline. Radiation patterns were normalized to the maximum co-polarization value obtained.

Figure 2.16 and Figure 2.17 present comparisons, at the particular frequency of interest, between the expected (finite ground plane) and measured results of the co-polarized E- and H-planes for the 1.3 GHz and 2.6 GHz antennas, respectively. The plots display good agreement between the simulated and measured radiation patterns. It is worth noting that the quarter-wavelength antenna only radiates from one edge. Therefore, the E-plane pattern becomes broader since the array effect of two radiating edges for a half-wavelength antenna is absent, [2].

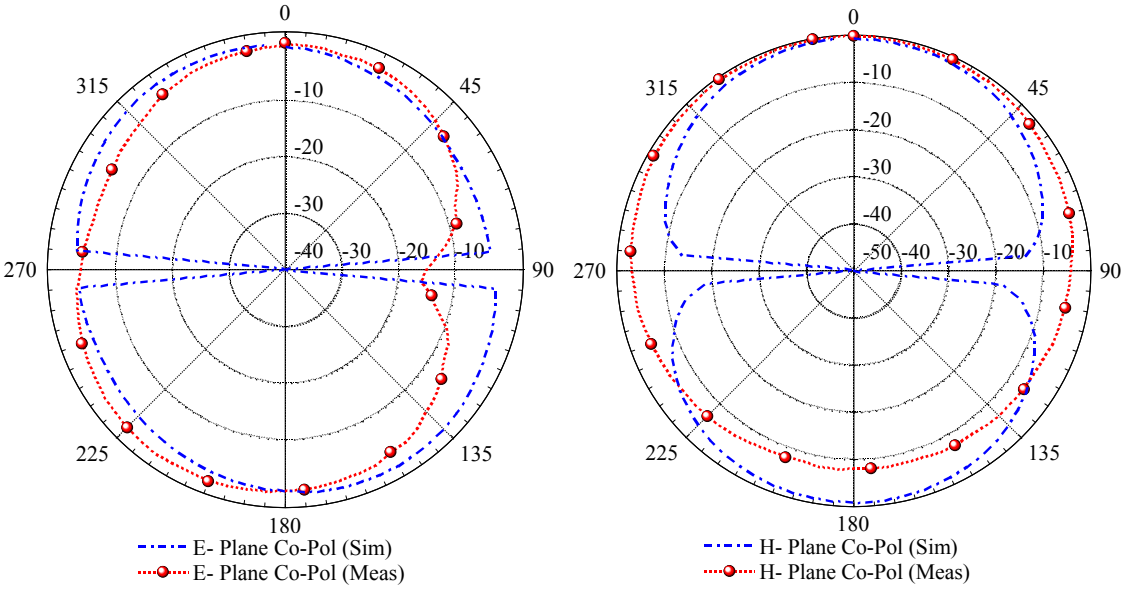

Figure 2.16: Comparison of Measured and Simulated Co-Polarized E-Plane (left) and H-Plane (right), Pattern of the 1.3 GHz Antenna, (dB)

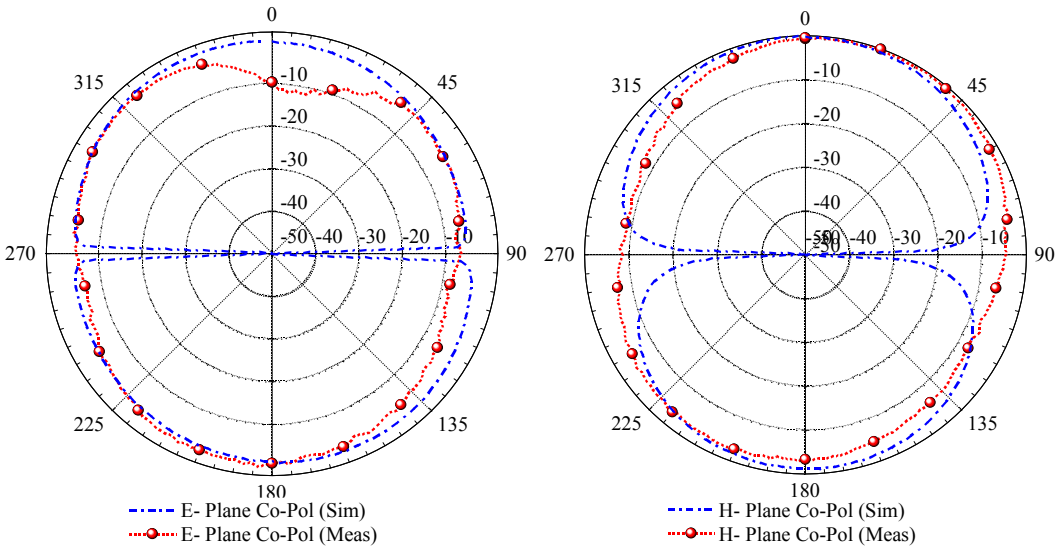

Figure 2.17: Comparison of Measured and Simulated Co-Polarized E-Plane (left) and H-Plane (right), Pattern of the 2.6 GHz Antenna, (dB)

Measured E- and H-plane cross-polarization patterns are presented in Figure 2.18. Measurements were normalized to the maximum co-polarization value obtained for each antenna.

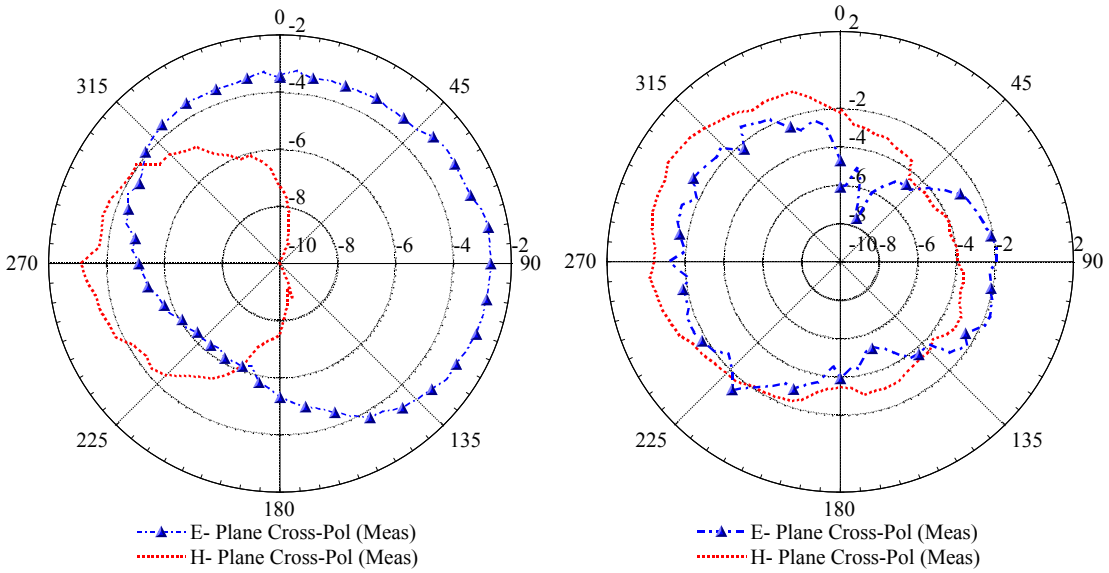

Figure 2.18: Cross-Polarized Measurement of the E and H-Plane Radiation Pattern, 1.3 GHz Antenna (left) and 2.6 GHz Antenna (right), (dB))

Considerable cross-polarization can be observed. Some possible causes for the cross-polarization levels are the lowered width to length ratio of the antenna and the utilization of a microstrip feed, which can increase these cross-polarization levels. Cross-polarization levels for shorted patch antennas have been reported to be higher than for half-wave patches, [2], [36]. Therefore, these compact microstrip antennas should be employed in applications where cross-polarization can be tolerated.

2.4 Power Measurement Techniques

On the transmitter side, a network analyzer was used to provide a continuous wave signal at 1.3 GHz and 0 dBm. This signal was further attenuated to different test levels using a variable attenuator. The signal was then amplified using an amplifier with a power output of 22 dBm. Two isolators, which operated at 1.3 GHz, were used to

ensure proper signal transmission at the proper frequency and to minimize any harmonic interference. A 20 dB coupler was used as a test point to observe the amplifier's drive level with the aid of a spectrum analyzer. Using a 3 dB power splitter, the 1.3 GHz signal was sent into a custom transmitting dual-patch array. The FDR was placed on a tripod in the anechoic chamber where it received the 1.3 GHz signal, doubled the frequency and transmitted it back a signal to a commercial 2.6 GHz Yagi tube antenna. A fabricated FDR device is displayed, fully assembled, in Figure 2.19.

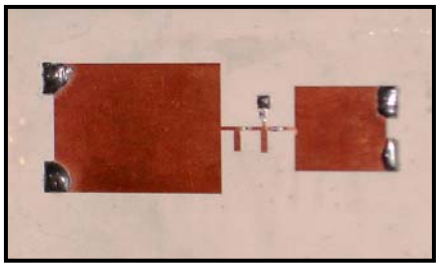

Figure 2.19: Fabricated Frequency Doubling Reflectenna

The received power transmitted by the harmonic re-radiator was measured using a spectrum analyzer. Path spreading losses were calculated using the free-space path loss formula

$$PL = 20 \times \log_{10}\left(\frac{4\pi d}{\lambda}\right) \text{dB}, \tag{2.3}$$

where d is the distance from the transmitter and λ is the signal wavelength. Both the distance and wavelength parameters are in meters.

The hardware test-bench utilized components and cables, which introduce loss into the system. Therefore, proper characterization of each element was performed to account for the losses being introduced. To validate the characterization for each of the

components of the system and the 1.3 GHz transmitting dual-patch gain, a preliminary test was conducted using a custom single 1.3 GHz patch antenna as the receiver. The power levels received by the patch antenna correlated with expected values for the power received. Once the validation was completed and an accurate measure conducted of the power received by the actual FDR, the single patch antenna was replaced by the FDR for testing.

Figures 2.20 presents a diagram of the test measurement setup utilized for the FDR tests.

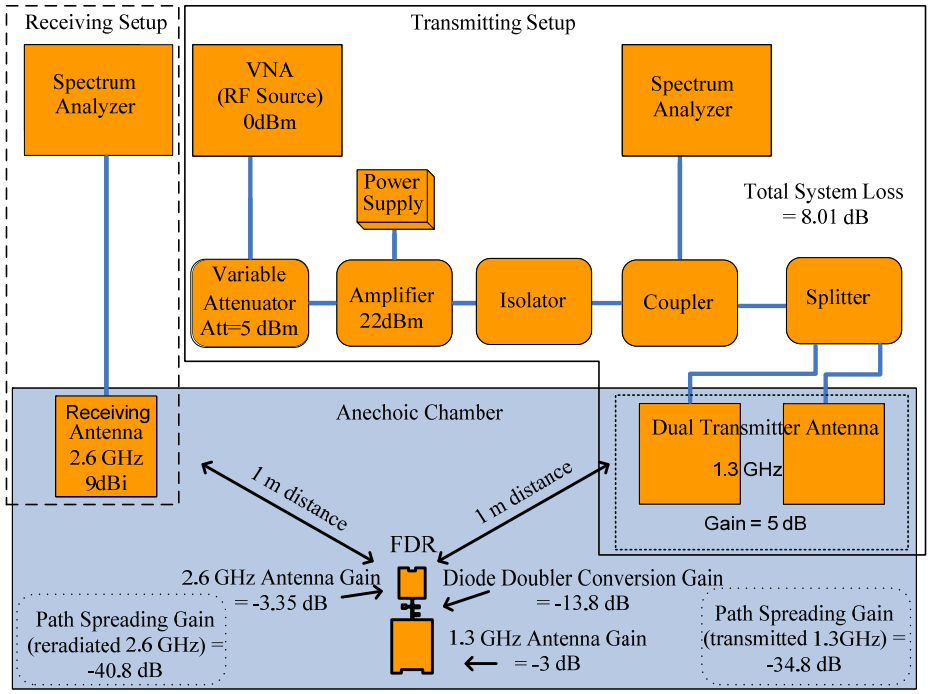

Figure 2.20: Diagram of the Harmonic Re-radiator Test Measurement Setup. The input power level to the FDR was -12.85 dBm

Figure 2.21 presents a picture of the complete arrangement utilized for performing measurements on the FDR.

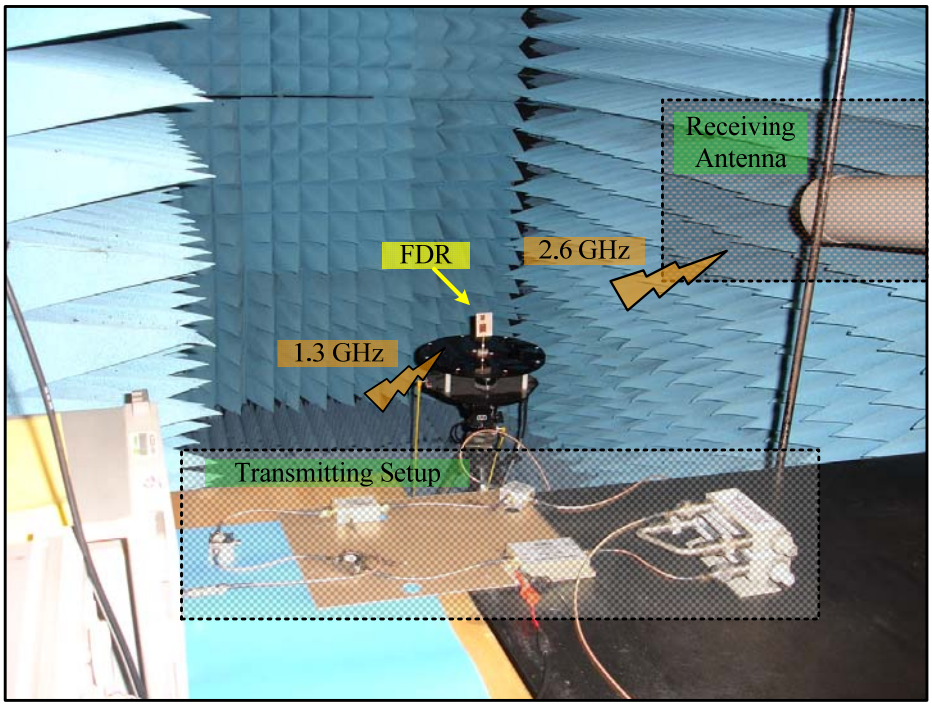

Figure 2.21: Hardware Test-Bench Used for FDR Measurements

The FDR was placed in an anechoic chamber where it received the transmitted 1.3 GHz signal. The FDR doubled the received signal frequency and re-radiated it at 2.6 GHz. Output power measurements are conducted using a spectrum analyzer, which was connected to the 2.6 GHz receiving antenna.

2.5 Results

The output power received at 2.6 GHz antenna and the multiplier conversion loss curves for three FDR's are presented in Figure 2.22. Conversion gain values were calculated by using the relationship

$$CG = P_{out}(dB) - P_{in}(dB) + Receiving\ system\ loss(dB). \quad (2.4)$$

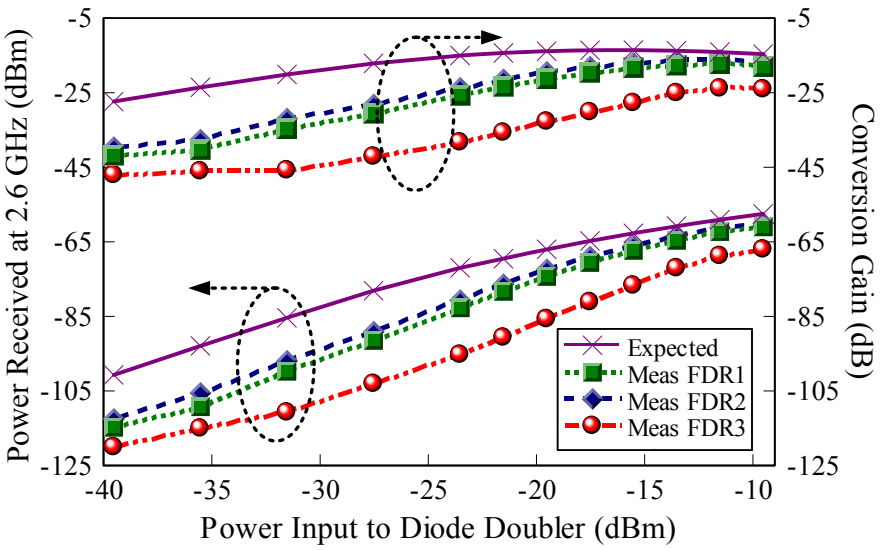

Figure 2.22: Comparison of Measured and Expected Output Power and Diode Doubler Conversion Gain at a Source Frequency of 1.3 GHz

Good correlation is demonstrated between the measured curves for FDR's 1 and 2. The received 2.6 GHz power for FDR 3 differed by approximately 7 dB from the other two re-radiators. Since the measured values differed from those obtained from simulation, the frequency sensitivity of the FDR was analyzed. Measurements were performed using source signals at frequencies close to 1.3 GHz with an input power to the FDR of -31.53 dBm. The results of the analysis are presented in Figure 2.23. The frequency at which the maximum doubler conversion efficiency occurred varied somewhat from 1.3 GHz for each sample.

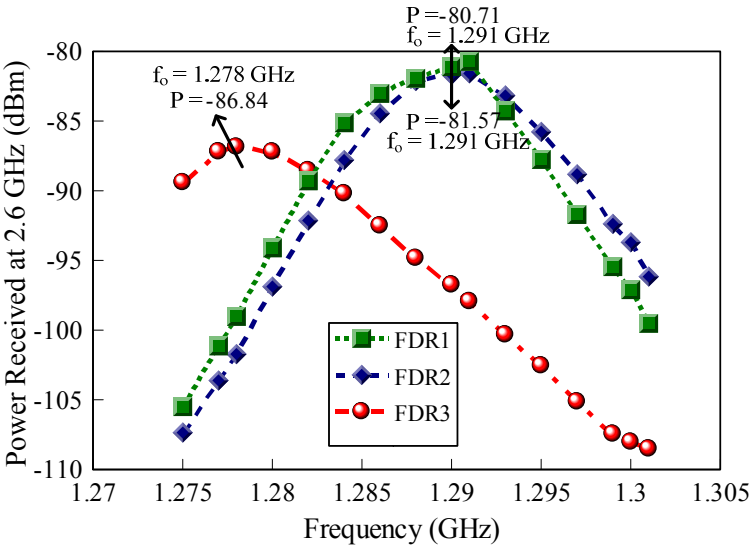

Figure 2.23: Measured Received Power for Different Source Frequencies. Diode Doubler Input Power was -31.53 dBm

Swept-power performance was measured at the source frequency that yielded the highest level of received power. This data was compared with the simulated data at a source frequency of 1.3 GHz. The comparison is presented in Figure 2.24.

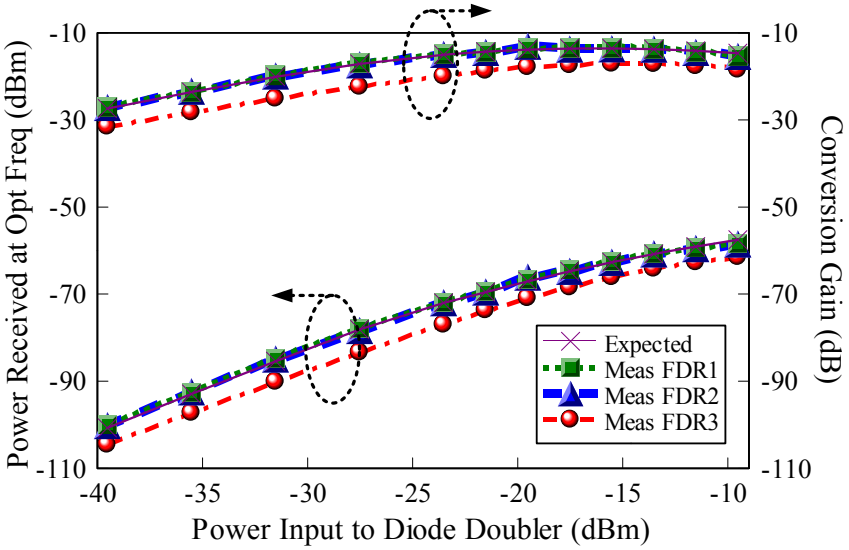

Figure 2.24: Comparison of Expected Doubler Conversion Gain and Output Power at a Source Frequency of 1.3 GHz and Measured Performance at the Fabricated FDR's Optimum Source Frequency

FDR's 1 and 2, demonstrated good agreement, a deviation of 0.7%, at a source frequency of 1.291 GHz. Peak power levels for FDR 3 occurred at 1.28 GHz, which was a deviation of 1.6%. The 1.3 GHz dual-patch array, see Figure 2.19, which was used as the transmit antenna possessed a narrowband response and provided less gain at 1.28 GHz than at 1.3 GHz. Over an input power range of -40 to -10 dBm, the FDR measured and simulated conversion gain of the doubler compared very well for FDR's 1 and 2. The conversion gain was -19.87 dB when the input power to the FDR was -31.53 dBm, and a maximum value of -13.7 dB for an input power of -15.53 dBm. These values are an improvement over what has been reported on a Schottky diode doubler/antenna transponder design, [17]. By considering the simulated value of gain of the input and output antennas, the measured conversion gain of the entire FDR's 1 and 2 at the optimum frequency of operation was -22.75 dB for an input power level at the FDR receiving antenna of -28.5 dBm. This FDR was designed for low-power input and zero-bias operation. In other frequency multipliers, where the input signal strength can be as high as 5 dBm, conversion loss values of close to10 dB are expected, [8].

2.6 Conclusions

A compact conjugate-matched frequency doubling reflectenna was designed, fabricated and tested. At an input frequency of 1.3 GHz a multiplier conversion efficiency of 1% was obtained at an input power of -30 dBm. A high degree of performance accuracy was obtained by the nonlinear simulations performed in the design process. The harmonic re-radiators were produced using careful, although not extremely precise, manufacturing methods with a small spread in performance. The conjugate-

matched design maximized conversion efficiency and increased the sensitivity of the design. Since the FDR's performance is relatively narrowband its operation could be controlled by using integrated control structures such as tuning capacitors. This FDR is a promising device for sensing applications.

CHAPTER 3

COMPACT PLANAR ANTENNAS: MEANDERED ANTENNAS

3.1 Introduction

The reduction of the size of wireless sensor devices is often desired due to the various applications in which they may be employed. In many wireless devices the antenna occupies the vast majority of the overall device area. This is the case with the FDR, where the receiving and transmitting antennas dominate the footprint of the design. Despite the work that has been conducted in miniaturized antennas, ongoing investigations are still prevalent since a reduction in the size of the antenna typically degrades its performance. In an integrated device with antennas, degraded antenna performance impacts the overall efficiency of the system. Therefore, studies, which aim to miniaturize the antenna without sacrificing parameters such as gain and efficiency, are important. Small antenna research often targets planar antennas due to their desirable light weight, low volume and conformal characteristics, [2], [36], [37].

In this chapter a brief review of important antenna parameters and a discussion of the fundamental limitations of electrically small antennas is presented. Some of the techniques, utilized by other authors, to miniaturize planar antennas are also mentioned. In order to produce a miniature harmonic re-radiator, two planar antenna designs were considered. A meandered slot antenna design and a meandered shorted patch antenna

design were investigated. A meandered slot antenna was designed for an operating frequency of 1.3 GHz. The meandered shorted patch antennas were designed for operating frequencies of 1.3 GHz and 2.6 GHz. The meandered shorted patch antenna provided an antenna size reduction of ~85% compared to the quarter-wavelength shorted patch antennas used in the first-generation FDR design. The gain of the miniature meandered patch antennas was optimized by increasing the substrate thickness without exceeding a value, which would allow the propagation of higher order modes.

3.2 Review of Antenna Parameters

Antennas can either convert an RF signal from a transmitter to a propagating electromagnetic wave or convert a propagating wave into an RF signal in a receiver. Therefore, antennas are reciprocal devices and the properties defined below apply either to an antenna utilized as a transmitting or a receiving device.

An antenna's radiation pattern is a plot of the transmitted or received signal strength versus position around the antenna. The operating frequency, the size and the gain are antenna parameters that are related to each other. An antenna needs to have minimum physical dimensions in order for effective radiation to occur. As the frequency of operation of an antenna increases its size decreases. In addition, since the gain of an antenna is proportional to its cross-sectional area divided by the wavelength squared, an electrically small antenna will usually have lower gain than a larger antenna, [38].

Wireless communications are possible due to the propagation of electromagnetic energy. An antenna converts a guided electromagnetic wave on a transmission line to a

plane wave propagating in free-space. The spherical coordinate system utilized in the analysis of antenna parameters is illustrated in Figure 3.1.

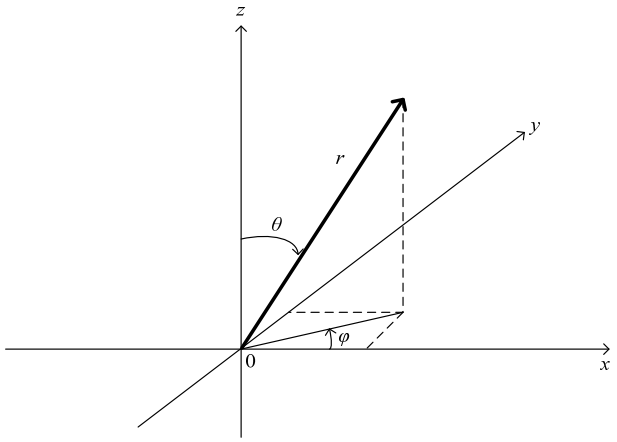

Figure 3.1: Spherical Coordinate System

The antenna radiates a spherical wave. However, at large distances this wave becomes an approximation of a plane wave. The distance where this occurs is referred to as the far-field distance. The far-field distance is defined as

$$R_{ff} = \frac{2D^2}{\lambda} \text{ m}, \tag{3.1}$$

where D is the maximum dimension of the antenna and λ is the wavelength.

In the far-field zone of the antenna, the radiated electric field is given by

$$\bar{E}(r,\theta,\phi) = [\hat{\theta} F_\theta(\theta,\phi) + \hat{\phi} F_\phi(\theta,\phi)] \frac{e^{-jk_o r}}{r} \text{ V/m} \tag{3.2}$$

where $\bar{E}$ is the electric field vector, $\hat{\theta}$ and $\hat{\phi}$ are unit vectors in the spherical coordinate system, r is the radial distance from the origin,

$$k_o = 2n\pi / \lambda, \tag{3.2a}$$

wavelength,

$$\lambda = c/f = 3\times10^8 / f\,, \tag{3.2b}$$

with frequency in Hz, and $F_\theta(\theta,\phi)$ and $F_\phi(\theta,\phi)$ are the pattern functions. The electric field propagates in the radial direction. The electric field may be polarized in either the θ or ϕ directions but not in the radial direction. Polarization of this type is characteristic of transverse electromagnetic, (TEM), waves. The magnetic fields associated with this TEM wave are given by

$$H_\phi = \frac{E_\theta}{\eta_0} \tag{3.3}$$

and

$$H_\theta = \frac{-E_\phi}{\eta_0} \tag{3.4}$$

where

$$\eta_0 = 377\ \Omega. \tag{3.4a}$$

The radiation pattern of an antenna denotes the magnitude of the far-zone field strength versus position around the antenna at a fixed distance. The field can be plotted from the pattern functions $F_\theta(\theta,\phi)$ and $F_\phi(\theta,\phi)$. The pattern functions depend on the

polarization of the antenna. If the pattern is plotted versus the angle θ it depicts an elevation plane pattern and if plotted versus the angle ϕ it depicts an azimuthal plane pattern.

The radiation intensity provides the variation in radiated power versus position around the antenna. Directivity provides a measure of the directionality of an antenna pattern or the focusing ability of an antenna. Directivity is defined as the ratio of the maximum radiation intensity in the lobe with the maximum value to the average radiation intensity over all space. Therefore, directivity is a dimensionless ratio of power, which is usually expressed in dB.

The antenna radiation efficiency was previously defined, in Chapter 2, in terms of the radiation resistance and the loss resistance. This definition does not take into account surface wave loss, which will be discussed in Section 3.6. The radiation resistance R_r is associated with the radiation of an antenna. Loss occurs in an antenna mainly due to dissipative losses in the metals and the dielectric materials used to fabricate the radiator. A reflection, (impedance), efficiency e_{ref} can also be described as a result of the reflections that arise due to the mismatch between the transmission line and the antenna. Reflection efficiency is given by

$$e_{ref} = (1 - |\Gamma^2|), \tag{3.5}$$

where

$$\Gamma = (Z_{in} - Z_0)/(Z_{in} + Z_0). \tag{3.5a}$$

The antenna input impedance is Z_{in} and the characteristic impedance of the line is Z_0. The overall efficiency is given by

$$e_o = e_{ref} e_{cd} . \tag{3.6}$$

Gain, related to an antenna, accounts for its losses and is defined as the product of directivity and efficiency. Antenna gain is usually expressed in dB and given by, [39]

$$G = e_{cd} D . \tag{3.7}$$

The bandwidth of an antenna is the range of frequencies on either side of a center frequency where the antenna characteristics are within an acceptable value of those at the center frequency. Input impedance is said to be the impedance presented by an antenna at its terminals, namely the input terminals of the antenna.

The polarization of an electromagnetic wave is defined as the orientation of the radiated electric field vector. For the case of a plane wave propagating along the z axis, the electric field may expressed as

$$\bar{E} = (E_{0x} \hat{x} + E_{0y} \hat{y}) e^{-jk_{0z}} . \tag{3.8}$$

When

$$E_{0x} = 1 \text{ and } E_{0y} = 0$$

the field is linearly polarized. When

$$E_{0x} = 1 \text{ and and } E_{0y} = 1$$

the field is linearly polarized in the 45˚direction in the $\hat{\phi}$ or azimuthal plane. Thus, the wave will be linearly polarized if both E_{0x} and E_{0y} have the same phase. In contrast, if E_{0x} and E_{0y} have a 90˚ shift, the field is said to be circularly polarized. If the magnitudes of E_{0x} and E_{0y} are not equal or the phase difference is not exactly 90˚, the field is said to be elliptically polarized. The polarization of the antenna will dictate the polarization of the radiated field, [38].

3.3 Limitations of Electrically Small Antennas

Since 1947, several studies have been reported on the fundamental limitations of electrically small antennas, [40 - 43]. Wheeler commented on the reduction of the radiation resistance, efficiency and bandwidth of a small antenna, [40]. In order to quantify the radiation of an antenna, Wheeler defined a radiation power factor that was equal to the antenna resistance divided by the antenna reactance. The radiation power factor for small antennas is less than one. With the purpose of further characterizing small antennas, Wheeler later defined the term radiansphere as a hypothetical sphere having a radius of $\lambda/2\pi$ from the center of an antenna, [44]. This sphere can be viewed as the space occupied by the stored energy of a small antenna's electric or magnetic field. As a result, a small antenna is one that occupies a small fraction of one radiansphere in space, [45]. An idealized small spherical antenna has a radiation power factor equal to the ratio of its volume to that of the radiansphere. Therefore, if an antenna is limited by a maximum dimension but not by an occupied volume, the radiation power factor can be increased by utilizing the volume of a sphere with a diameter equal to this maximum dimension, [44].

Chu described the performance of an antenna in terms of its power gain and its bandwidth. He defined the largest linear dimension of the antenna to be $2r$, such that the complete antenna structure is enclosed inside a spherical surface of radius r. The quality factor Q is directly proportional to the mean electric energy stored beyond the input terminals of the antenna times 2ω divided by the power dissipated in radiation. Moreover, the bandwidth of the antenna is indirectly proportional to Q. In addition, Chu found that if the Q of an antenna is required to be low, there is a definite limit to the gain of a practical antenna that is approximately equal to $4r/\lambda$, [41].

The concept of an antenna enclosed in a sphere of radius r was also utilized by Hansen and is illustrated in Figure 3.2. Hansen defined $k = 2\pi/\lambda$ and explained that higher modes may not be present for $kr < 1$. For $kr << 1$, Q varies inversely as the cube of the radius of the sphere. The radiation Q increases rapidly as the size of the antenna decreases, [42].

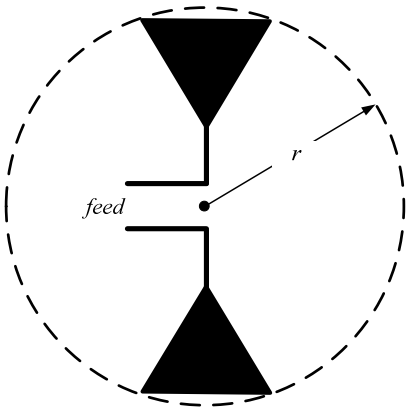

Figure 3.2: Antenna Within a Sphere of Radius r, [42]

Mclean derived an exact expression for the radiation Q associated with the TM_{01} mode, which is given by

$$Q = \frac{1}{k^3 r^3} + \frac{1}{kr}. \tag{3.9}$$

If $kr << 1$ equation (3.9) reduces to

$$Q = \frac{1}{k^3 r^3}. \tag{3.10}$$

A circularly polarized antenna, given by a combination of TE_{01} and TM_{01} modes, will yield the lowest achievable radiation Q and will be approximately half that of a linearly polarized antenna. In addition, a narrower maximum achievable bandwidth is obtained with a larger radiation Q, [43].

Recently, additional studies have been conducted on the quality factor of electrically small antennas, [46 -48]. Best found that the quality factor of an electrically small wire antenna is mainly determined by the antenna's height and effective volume in relation to the resonant wavelength, [48]. Therefore, modifying the geometry of an antenna within a fixed height and fixed cylindrical diameter does not significantly improve the performance of a small self-resonant antenna. A small antenna, which Best defined as one with a boundary limit at $kr = 0.5$, usually has a radiation resistance that is very low and an input reactance that is very high, [47]. Essentially, the best compromise between bandwidth and efficiency will usually be achieved when most of the allotted volume in an antenna design is utilized in radiation, [49].

3.4 Size Reduction Techniques for Planar Antennas

Miniaturizing techniques utilized to reduce the size of different types of antennas consist primarily of loading the antenna with lumped elements, of utilizing high-dielectric materials or conductors and use of the antenna casing to increase radiation. A small antenna will usually have a high input reactance, which can be compensated by lumped-element loading. This method will either reduce the efficiency of the antenna or increase its quality factor. In addition, an antenna may be miniaturized by altering the dielectric or magnetic characteristics of the encasing material. However, modification of the encasing material can reduce the bandwidth of the antenna and produce higher dielectric losses. An antenna's overall physical size can also be reduced by modifying its geometry and shape, [49].

The desire for smaller mobile communication devices has enabled some of the advances in the area of compact planar antennas. Effective methods utilized to design miniature antennas, which do not exhibit degraded gain or cross-polarization, have been reported. Several authors have presented comprehensive reviews of compact microstrip antennas, [2], [36], [37].

Planar antennas such as microstrip antennas, printed monopole and dipole antennas and slot antennas have been studied extensively. These types of antennas, except for the printed monopole, are illustrated in Figure 3.3.

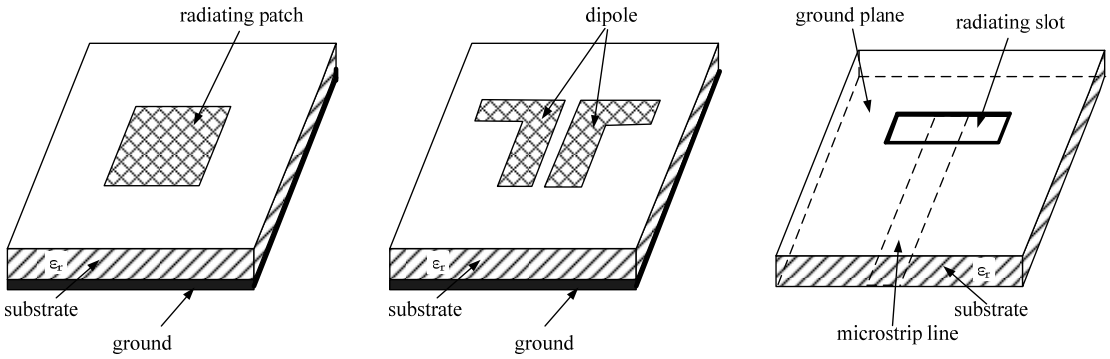

Figure 3.3: Configuration of Different Planar Antennas:
Microstrip Patch (left); Printed Dipole (middle);
Slot Antenna (right), [2]

A microstrip antenna may simply consist of a radiating patch of metallization on a grounded dielectric substrate. Microstrip antennas are characteristically light weight, low-profile and low-cost. However, they may be limited by a narrow-bandwidth, lower gain and poor efficiency. Printed dipoles can be considered as narrow rectangular patches. Printed slot antennas are those, which consist of a slot in the ground plane of a grounded substrate. Printed slot antennas can be fed by a microstrip line or a coplanar waveguide, [2].

As with the shorted patch antennas described in Chapter 2, other edge-shorted rectangular patch antennas have also been reported. The quarter-wavelength antennas described in the previous chapter utilized shorting vias to reduce the antenna size. However, structures employing shorting walls or shorting plates instead of via holes have been developed. When a shorting pin is loaded at the tip of an equilateral-triangular microstrip antenna, its size can be reduced by as much as 94%, [50].

Size reduction is also achieved by introducing several slits in the non-radiating edges of a rectangular patch antenna. The slits create an effect where the patch's surface

currents are effectively meandered. Therefore, the current path is lengthened, which reduces the antenna's resonant frequency, [51]. Similarly, a bow-tie patch has been designed by cutting triangular notches at both non-radiating sides of the patch. Surface current path lengthening can also be achieved by utilizing three dimensional structures such as the U-shaped patch, the folded patch or the double-folded patch, which is termed a planar inverted-f. The patch's surface current is bent along the antenna's resonant dimension and no lateral currents are generated, thereby reducing cross-polarization levels.

Rectangular patches that contain embedded slots have been implemented to produce compact antennas. Slot geometries can range from cross slots, rectangular slots and circular slots. These slots cause meandering of the patch surface currents, which is an effect that generates compact antenna designs. Compact microstrip antennas exhibiting dual-frequency operation have also been realized. These designs achieve their effect by embedding a pair of slots parallel and close to the radiating edges of a meandered rectangular antenna or a bow-tie patch. A miniature dual-band folded patch antenna has been proposed, [52].

As mentioned in the previous section, the gain and efficiency characteristics of an antenna might degrade as the physical size of the structure decreases. Therefore, several techniques have been implemented in order to increase the gain of compact microstrip antennas. These include utilizing a high-permittivity dielectric superstrate or integrating active circuitry into the antenna structure. Both techniques have been found to increase the gain of the antenna, [53 - 56].

3.5 Meandered Slot Antenna

In order to reduce the overall footprint of the FDR design, a meandered slot antenna was considered as an alternative design to the quarter-wavelength shorted patch antenna. The slot antenna geometry provides several advantages over the quarter-wavelength shorted patch antennas. Employing a coplanar waveguide, (CPW), fed slot antenna alleviates the shortcomings on the radiation efficiency created by the shorted patch antenna's via resistance. The geometry of a basic CPW-fed slot antenna employing a center feed is illustrated in Figure 3.4.

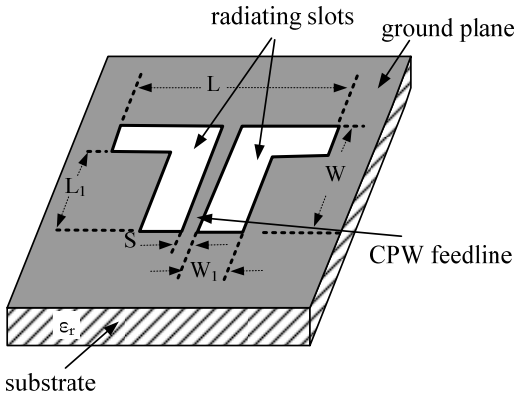

Figure 3.4: CPW-Fed Slot Antenna, (Design A)

Table 3.1 presents the parameters for antenna Design A, which is illustrated in Figure 3.4.

Table 3.1: Parameters for a Half-Wavelength CPW-Fed Slot Antenna Design (Dimensions in Millimeters)

Design	**L / W**	**L_1 / S / W_1**
A	64 / 2	1.5 / 1 / 0.5

Slot antennas can be less sensitive to tolerances due to manufacturing and can be polarized in a certain way using a combination of strip and slot conductors, [2]. Meandering or folding a slot antenna can further reduce its size. Use of a CPW line to feed the slot antenna is useful in the design since mutual coupling between adjacent lines is minimized, [2]. Therefore, meandered slot antennas can be placed in close proximity, which reduces the physical size of the overall circuit. In addition, a center-fed slot antenna has a very high radiation resistance.

Agilent's Momentum was used to analyze antenna characteristics such as return loss, input impedance and gain. A traditional CPW-fed slot antenna such as the one presented in Figure 3.4 was designed to be approximately half-wavelength at the desired operating frequency of 1.3 GHz. The board substrate employed for the design was 60 mil Taconic, ($\varepsilon_r = 6.15$). Analysis of the properties of this traditional geometry, which was designated Design A, was conducted with the purpose of providing a baseline for analysis of subsequent meandered slot geometries. The meandered slot geometry investigated in this research and designated Design B is illustrated in Figure 3.5.

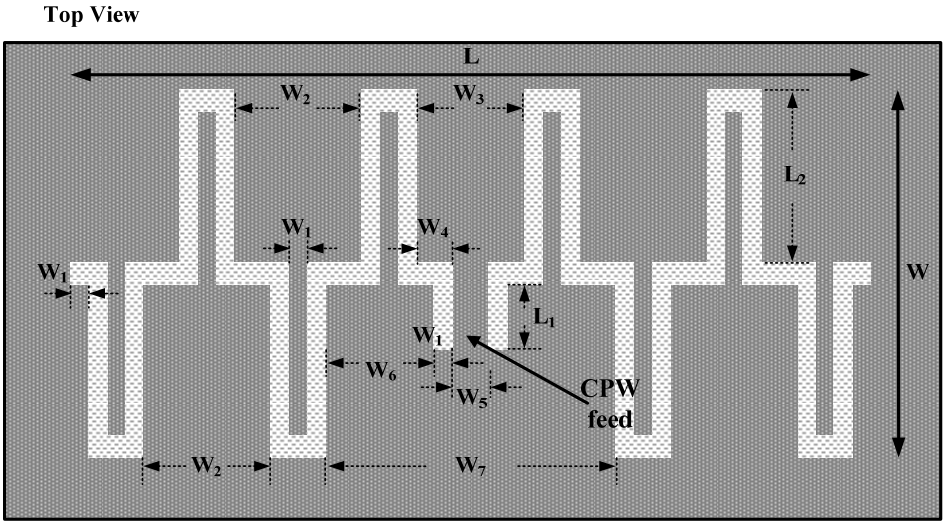

Figure 3.5: CPW-Fed Meandered Slot Antenna (Design B)

Table 3.2 presents the parameters for antenna Design B, which is illustrated in Figure 3.5.

Table 3.2: Parameters for Meandered Slot Antenna Design (Refer to Figure 3.5)
(Dimensions in Millimeters)

Design	**L / W**	**L_1 / L_2 / W_1 / W_2 / W_3 / W_4 / W_5 / W_6**
B	22 / 8.5	1.5 / 4 / 0.5 / 3.5 / 3 / 1 / 1 / 3

When compared to the basic slot antenna design, the size reduction obtained in the total length of the antenna with the meandered slot antennas geometry was 65.6% for Design B. Additional meandered slot geometries investigated in this research and designated Design C, Design D and Design E are illustrated in Figure 3.6.

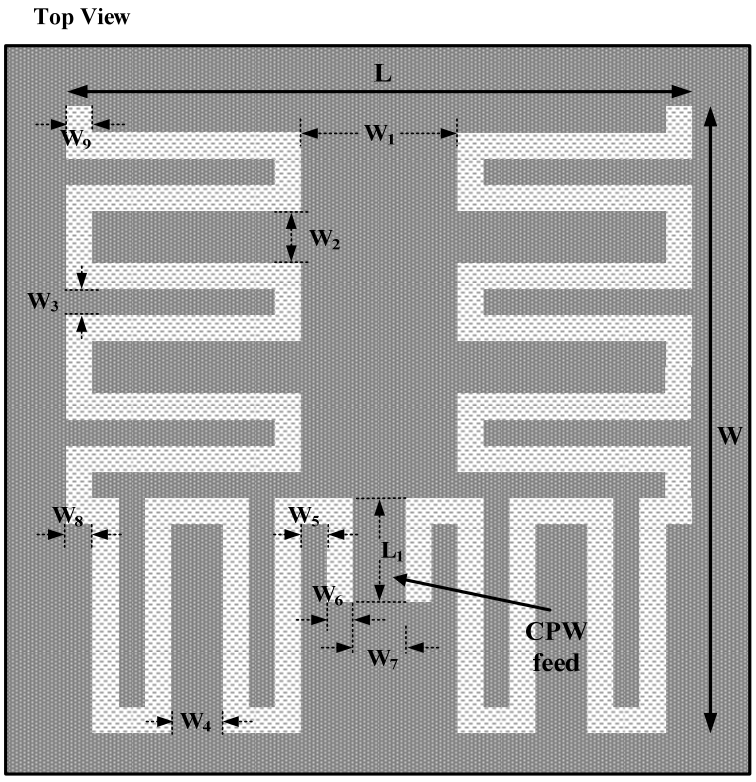

Figure 3.6: CPW-Fed Meandered Slot Antenna (Designs C, D, E)

Table 3.3 presents the parameters for antenna Designs C, D and E, which are illustrated in Figure 3.6.

Table 3.3: Parameters for the Meandered Slot Antenna Design (Refer to Figure 3.6) (Dimensions in Millimeters)

Design	**L / W**	**L_1 / W_1 / W_2 / W_3 / W_4 / W_5 / W_6 / W_7 / W_8 / W_9**
C	12 / 12	2 / 3 / 1 / 0.5 / 1 / 0.5 / 0.5 / 1 / 0.5 / 0.5
D	11.5 / 12	2 / 2.5 / 1 / 0.5 / 1 / 0.5 / 0.5 / 0.5 / 0.5 / 0.5
E	9 / 10.25	2 / 1 / 0.5 / 0.5 / 0.5 / 0.5 / 0.5 / 1 / 0.25 / 0.25

When compared to the basic slot antenna design, the size reduction obtained in the total length of the antenna with the meandered slot antenna geometry was 81.2% for Design C. The physical dimensions of the meandered slot antenna were optimized utilizing the electromagnetic simulator. The dimensions obtained for the meandered slot antenna designs C – E represent a reduction of ~ 50% when compared to the 1.3 GHz shorted patch antenna described in Chapter 2.

Simulation results of the return loss; both magnitude and phase, of the five slot antenna designs considered were obtained. Figure 3.7 presents a comparison plot for the magnitudes and Figure 3.8 presents a comparison plot for the phases.

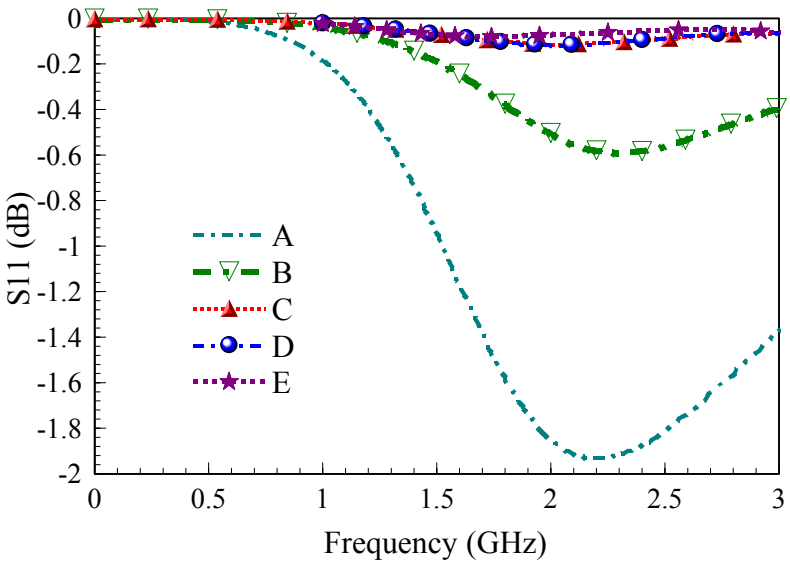

Figure 3.7: Simulated S11, (Magnitude), of CPW-Fed Slot Antenna Designs A - E

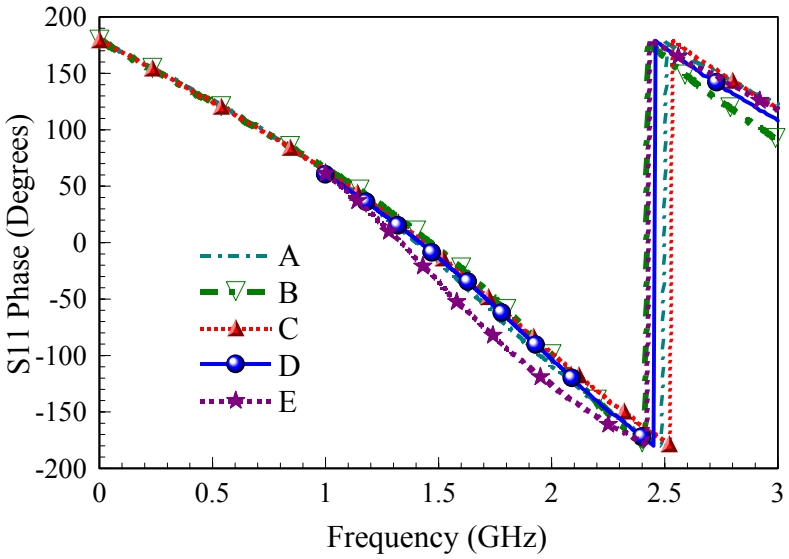

Figure 3.8: Simulated S11, (Phase), of CPW-Fed Slot Antenna Designs, A - E

It is important to observe that when calculating the values for the magnitude of S11, the simulator considered the design to be matched to 50 Ω. The input impedance of the antenna designs was not 50 Ω. Therefore, the values displayed in Figure 3.7 are low for most designs. The input impedances for the five designs were simulated and are presented in Figures 3.9 and 3.10. A comparison plot of the real part of the input impedance for the designs investigated is presented in Figure 3.9. The imaginary part of the input impedances is presented in the comparison plot of Figure 3.10.

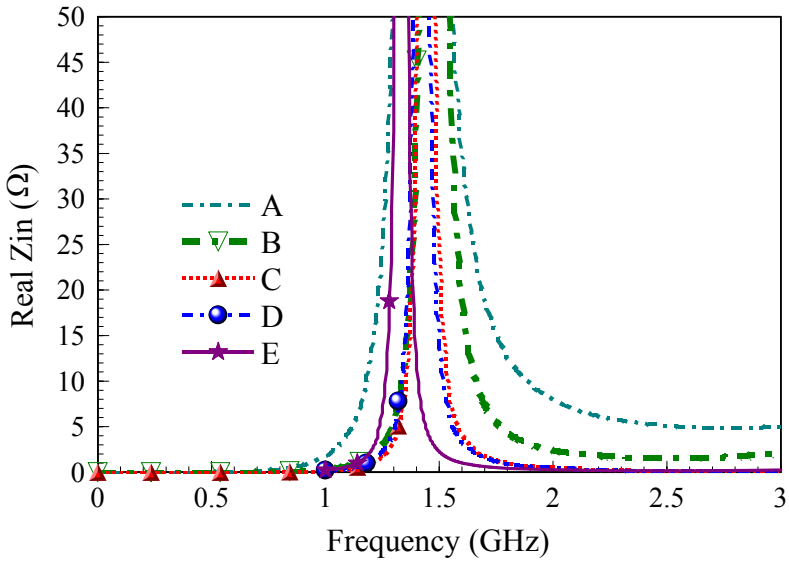

Figure 3.9: Simulated Real Input Impedance for CPW-Fed Slot Antenna Designs, A – E

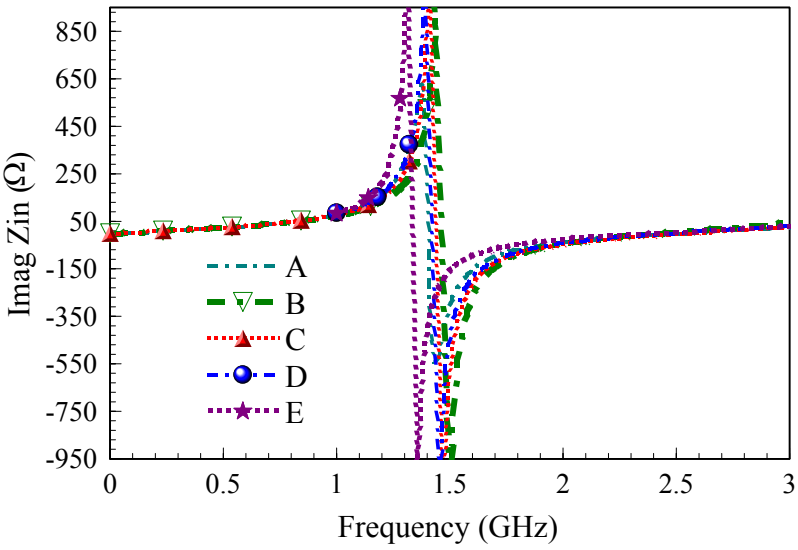

Figure 3.10: Simulated Imaginary Input Impedance for CPW-Fed Slot Antenna Designs, A – E

The simulated E- plane patterns of the five slot antenna designs are presented in Figure 3.11. It can be observed that the meandered slot designs present radiation patterns similar to the ones of the traditional CPW-fed slot antenna.

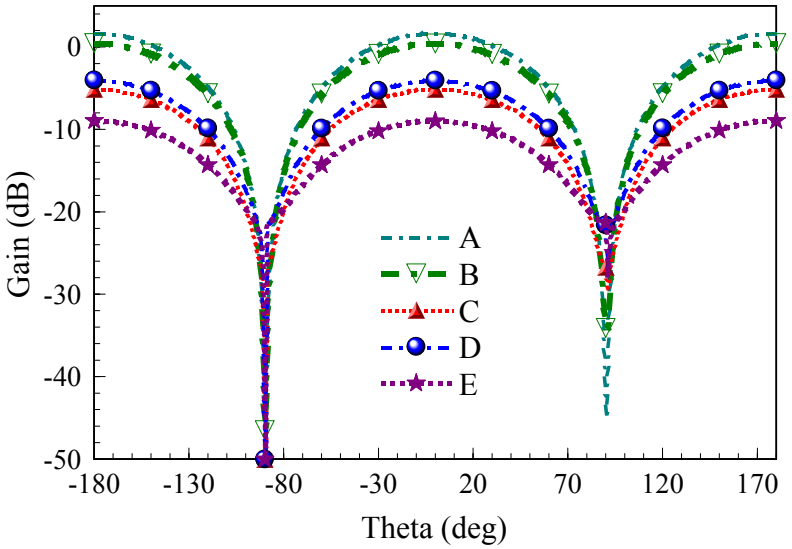

Figure 3.11: 1.3 GHz Simulated E- Plane Patterns for CPW-Fed Slot Antenna Designs, A – E

The values for the resonant frequencies of the different antenna geometries studied are presented in Table 3.4.

Table 3.4: Parameters for Slot Antenna Designs
(Refer to Figures 3.4 -3.6)

Design	L / W (mm)	f_o (GHz)
A	64 / 2	1.4
B	22 / 8.5	1.446
C	12 / 12	1.439
D	11.5 / 12	1.417
E	9 / 10.25	1.336

In order to produce an antenna design that would resonate at a frequency close to that of Design A, the total length of the meandered slot for Designs B – E was slightly larger than the total length of the slot for Design A. However, the increase in the total length of the meandered slot did not significantly increase the overall size of the antenna geometry, (refer to Tables 3.1 – 3.3).

A comparison of the simulated input impedance, gain and efficiency for the different slot antenna geometries investigated is presented in Table 3.5.

Table 3.5: Parameters for Slot Antenna Designs
(Refer to Figures 3.4 -3.6)

Design	L / W (mm^2)	Re {Zin} / Im {Zin} (Ω)	Gain (dB)	Efficiency (%)
A	64 / 2	62.0 / 303.9	1.7	94.3
B	22 / 8.5	6.0 / 218.2	0.4	72.2
C	12 / 12	3.6 / 261.3	-3.5	30.0
D	11.5 / 12	5.2 / 310.5	-3.7	28.8
E	9 / 10.25	49.9 / 908.9	-9.0	8.5

The meandered slot antenna designs exhibited low real input impedance values when compared to a basic CPW-fed slot antenna. Meandering of the slot did not result in a significant decrease of the antenna efficiency for Design B. A decrease in the efficiency for Designs B – E was observed. For the meandered slot geometry illustrated in Figure 3.6, decreasing parameters such as the width of the slot and the separation between meandered sections resulted in a decrease in the gain of the antenna.

Integrating a CPW-fed antenna into the FDR design would have resulted in having to re-design the layout for the harmonic re-radiator. CPW-to-microstrip transitions would have had to be studied and implemented. Additionally, implementing slot antennas into the design would have lead to a change in the radiation pattern from unidirectional to bidirectional. For ease in the design methodology, a shorted meandered patch antenna design was eventually chosen for a second-generation FDR design. This compact microstrip antenna design is described in the next section.

3.6 Meandered Shorted Patch Antenna

3.6.1 Antenna Design

In general, for a rectangular patch operating in the fundamental TM_{10} mode and designed for a thin dielectric, the length L should be

$$L \cong \frac{c}{2f\sqrt{\varepsilon_r}} \tag{3.11}$$

where c is the speed of light, f is the resonant frequency and ε_r is the relative permittivity of the substrate, [37]. If the patch is operating in the fundamental TM_0 mode, then the field varies every $\lambda/2$ along the length and no variation occurs along the width of the antenna. Lowering of the fundamental resonant frequency has been achieved by meandering the excited patch surface current paths in the radiating patch, [37]. The meandering leads to an extended current path for a fixed length. Thus, a meandered shorted patch antenna was devised from the design of the quarter-wavelength shorted patch antennas used in the first-generation FDR design.

The total length of the meandered shorted patch antenna was calculated using equation (3.11). In the same manner as with the quarter-wavelength antenna described in Chapter 2, shorting vias were used to decrease the size of the patch from a half-wave to a quarter-wavelength. The total length of the antenna corresponding to a quarter-wavelength was meandered in different sections. A study was conducted on the correlation between the number of meandered sections for a meandered patch antenna and its resonant frequency, [54]. Utilizing the findings of the Lancaster study and considering the difference between the antenna substrate utilized, an initial number of

five meandered sections was used. The number of meandered sections was optimized using the electromagnetic simulator to produce an antenna with the desired response.

The design method used for these meandered shorted patch antennas was similar to the one used for the quarter-wavelength shorted patch antennas of the first-generation FDR design. The meandered shorted patch antennas were initially designed so that their lowest resonance occurred approximately when the total length of the meandered line was a quarter-wavelength. The real impedance of the first-generation quarter-wavelength shorted patch antennas was optimized to be on the order of 40 Ω. As discussed in the previous sections, as the electrical length of an antenna decreases, so does its radiation resistance and efficiency. This effect was observed in the performance results obtained from initial antenna simulations. The input resistance of the meandered shorted patch antenna was much lower than the intended value of 40 Ω. As the real input impedance of the antenna increased, the antenna efficiency decreased. Using equation (2.2) from Chapter 2, the reduction in antenna efficiency indicated that a higher value of real input impedance was due to an increment in loss resistance R_L, which was undesirable.

Since a compact microstrip antenna will yield low efficiency values, special attention was given to obtaining the maximum efficiency possible for the meandered shorted patch antennas. It has been reported that gain and efficiency for a shorted patch antenna is less than those for a half wave patch antenna, [2]. This reduction in efficiency is intensified due to the small dimensions of the meandered shorted patch antenna as discussed in Section 3.3.

As reported by Best, an electrically small antenna will have a low radiation resistance and a high input reactance, [47]. Thus, efforts were made to optimize the

design in order to minimize the input reactance and maximize the input resistance without degrading the antenna efficiency.

Several physical antenna parameters were optimized to obtain the desired antenna parameters with the aid of the *ADS Momentum* electromagnetic simulator. The optimized parameters included:

- the total length of the meander line of the antenna,
- the number and location of shorting vias,
- the number of meandered sections,
- the slot size between sections,
- the width of the meander line,
- the total length and width of the structure,
- the geometry, dimensions and location of the feedline.

In an attempt to reduce the overall loss resistance, the antenna was shorted with a set of two parallel vias. It has been noted that, a single short at the corner of the antenna creates the most compact design for a rectangular patch antenna. The vias on the meandered shorted patch antennas were located in the corner of the non-radiating edge of the antenna opposite to the feedline for the 1.3 GHz antenna, [36]. Figure 3.12 illustrates the geometry for the 1.3 GHz meandered shorted patch antenna.

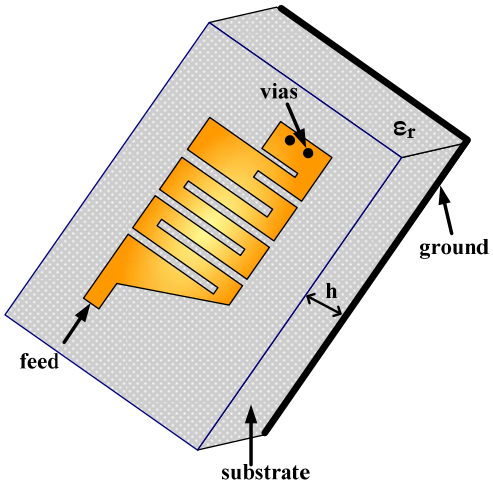

Figure 3.12: Geometry of the Meandered Shorted Patch Antenna, (1.3 GHz Design)

Table 3.6 presents the final parameters for the design of each of the antennas.

Table 3.6: Parameters for 1.3 GHz and 2.6 GHz Meandered Shorted Patch Antenna Designs of Figure 3.13 (Dimensions in Millimeters)

Design	**L / W**	**L_1 / L_2 / L_3 / L_4 / L_5 / L_6 / L_7 / W_1 / W_2 / W_3 / W_4**
1.3 GHz Antenna	5.05 / 10.54	1.05 / 0.26 / 0.14 / 0.40 / 0.80 / 0.27 / 2.0 / 1.69 / 2.3 / 0.50 / 0.50
2.6 GHz Antenna	11.5 / 12	1.05 / 0.26 / 0.15 / 0.30 / 0.25 / 0.25 / 1.5 / 1.69 / 1.4 / 0.50 / 0.50

Figure 3.13 provides a layout for both the 1.3 GHz and the 2.6 GHz designs, which indicates the locations of the parameters provided in Table 3.6.

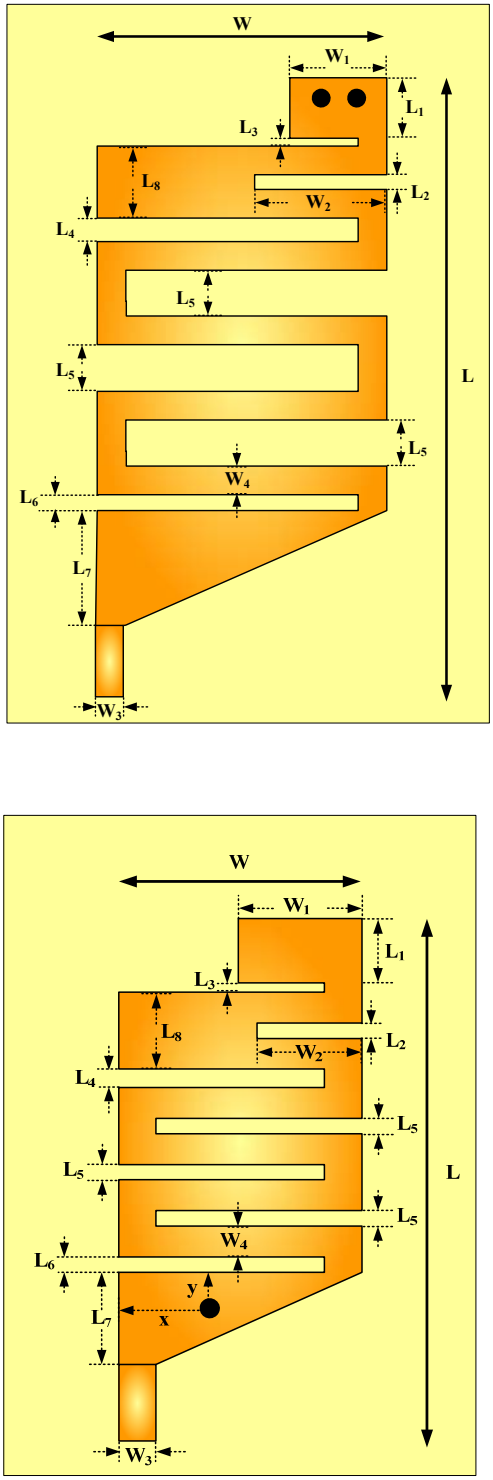

Figure 3.13: 1.3 GHz, (top), and 2.6 GHz, (bottom)
Meandered Shorted Patch Antennas
(at 2.6 GHz; via at x = 1.3 mm and y = 0.5 mm)

Figure 3.14 presents a comparison plot between the measured and simulated S11 data, referenced to 50 Ω, for the 1.3 GHz antenna.

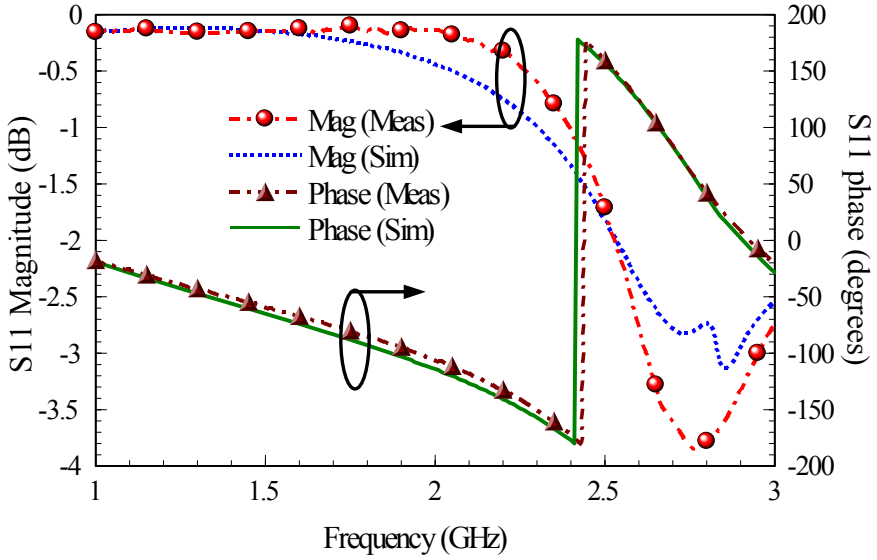

Figure 3.14: Comparison of Measured and Simulated S11 of the 1.3 GHz Antennas

Figure 3.15 presents a comparison plot between the measured and simulated S11 data, referenced to 50 Ω, for the 2.6 GHz antenna.

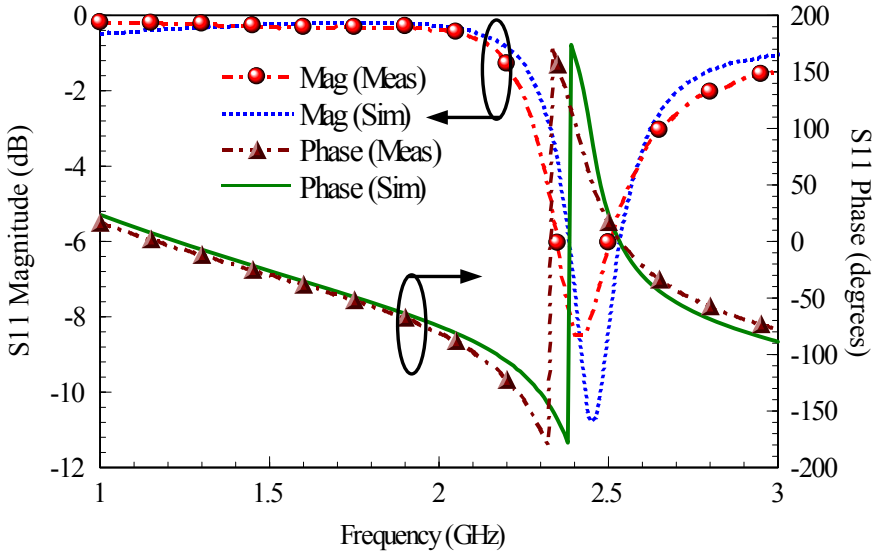

Figure 3.15: Comparison of Measured and Simulated S11 of the 2.6 GHz Antennas

Section 2.3.1 describes the procedure utilized to obtain return loss measurements and the process used to obtain a model to properly perform simulated and measured response comparisons. The expected S11 data was obtained by assuming an infinite ground plane since the excitation ports available in the simulator yielded more accurate return loss values compared to using excitation ports defined for a finite ground plane.

Plots of the simulated input impedance as a function of frequency are presented for both the 1.3 GHz and 2.6 GHz, meandered shorted patch antennas in Figure 3.16.

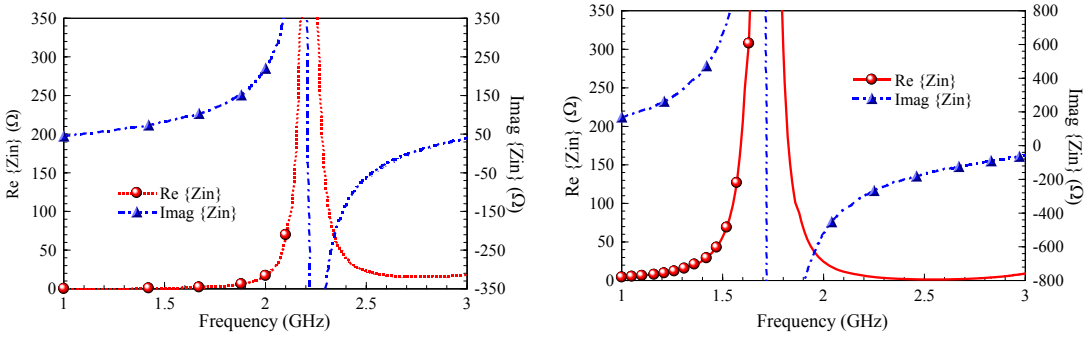

Figure 3.16: Plot of Simulated Input Impedance vs. Frequency for Meandered Shorted Patch Antennas: 1.3 GHz (left) and 2.6 GHz (right)

It is important to observe that in order to obtain the desired input impedance for the 2.6 GHz antenna a via was placed near the feed of the antenna. The resulting 1.3 GHz antenna had an input impedance of (12.7 + j335) Ω and the 2.6 GHz antenna had an input impedance of (19.3 + j25.15) Ω.

3.6.2 Substrate Thickness and Antenna Efficiency Considerations

Antenna electromagnetic simulations revealed that increasing the substrate thickness from 1.524 mm to 7.874 mm increased the simulated efficiency and gain of the meandered shorted patch antenna. Therefore, an analysis on the effects of this significant

increase in substrate thickness on the performance parameters of the antenna was performed. Since microstrip antennas can be considered lossy cavities, they can be modeled using a cavity model. The principal assumption for this model is that the substrate thickness

$$h << \lambda_0.$$

The model was applied to several patch shapes including rectangular patches. The interior region of the patch is considered a cavity bounded by electric walls on the top and the bottom with a magnetic wall along the edge. The meandered patch antenna can be considered a rectangular patch with slits. Therefore, the cavity model relationships can also be applied to the meandered patch antenna, [2]. The following analysis is derived from utilizing cavity model relationships.

Surface waves are excited on microstrip antennas if the substrate has an $\varepsilon_r > 1$. The surface wave is launched into the substrate where it can be reflected back and diffracted by the edges. Surface waves are TM and TE modes of the substrate. The lowest TM mode, the TM_0 mode, has no cutoff frequency. The value of the substrate thickness determines that only the TM_0 surface wave propagates. In order to allow the TM_0 surface wave mode to propagate and avoid the excitation of other modes, the relationship

$$\frac{h}{\lambda_0} < \frac{1}{4\sqrt{\varepsilon_r - 1}} \tag{3.12}$$

must be satisfied. In equation (3.12), h is the thickness of the substrate, λ_o is the waveguide wavelength in free-space and ε_r is the relative permittivity of the substrate. For the meandered shorted patch antenna designs

$$h = 7.874 \text{ mm}$$

and equation (3.12) was satisfied for both the 1.3 GHz and 2.6 GHz antennas. Thus, only the TM_0 mode surface wave propagated through the substrate.

A thicker substrate increases the radiated power and reduces conductor loss. However, it might also increase dielectric loss and surface wave loss, [2]. The power lost in the lossy dielectric of the substrate is denoted by, P_d. The power lost due to the finite metallization conductivity is denoted by P_c. The power radiated in the form of a space wave is denoted by, P_r.

The dielectric loss is given by

$$P_d = \omega \cdot \tan\delta \cdot W_t \tag{3.13}$$

where tanδ is the loss tangent of the dielectric, and W_T is the energy stored at resonance. The conductor loss is given by

$$P_c \approx \frac{\omega W_T}{h\sqrt{\pi f \mu_0 \sigma}} \tag{3.14}$$

where σ is the conductivity of the conductor. Equation (3.14) indicates that P_c decreases with increasing substrate thickness h, [2]. The power radiated from the patch, P_r, is determined by integrating the radiation field over the hemisphere above the patch using

$$P_r = \frac{1}{2\eta_0} \int_0^{2\pi} \int_0^{\frac{\pi}{2}} (|E_\theta|^2 + |E_\phi|^2) r^2 \sin\theta d\theta d\phi . \quad (3.15)$$

In equation (3.15), E_θ and E_Φ are complicated functions of θ, Φ and substrate parameters.

The total quality factor of the antenna can be approximated by

$$Q_T \approx \frac{\omega_r W_T}{P_r} . \quad (3.16)$$

In addition,

$$W_T \propto h\varepsilon_r \quad (3.17)$$

and

$$P_r \propto h^2 . \quad (3.18)$$

Therefore,

$$Q_T \propto \varepsilon_r / h . \quad (3.19)$$

From equations (3.16) and (3.19) and given that the total power loss, P_T, is inversely proportional to Q_T, it follows that the total power loss may be reduced by increasing the substrate thickness h.

An analysis of the impact of substrate thickness on the antenna radiation efficiency follows. It is important to point out that authors often define antenna radiation efficiency as the ratio of power radiated to the sum of radiated power and surface wave

power, [2], [57]. This definition neglects power dissipated in the conductor and dielectric. The antenna radiation efficiency can be expressed as

$$e_r = \frac{P_r}{P_i} = \frac{P_r}{P_r + P_c + P_d + P_{sur}} \tag{3.20}$$

where P_{sur} is the power loss associated with the surface waves. If

$$P_c + P_d \approx 0,$$

then

$$e_r \approx \frac{P_r}{P_r + P_{sur}}. \tag{3.21}$$

Expected E-plane patterns for three substrate thicknesses of the Taconic substrate, (ε_r = 6.15), for the 1.3 GHz antenna are presented in Figures 3.17

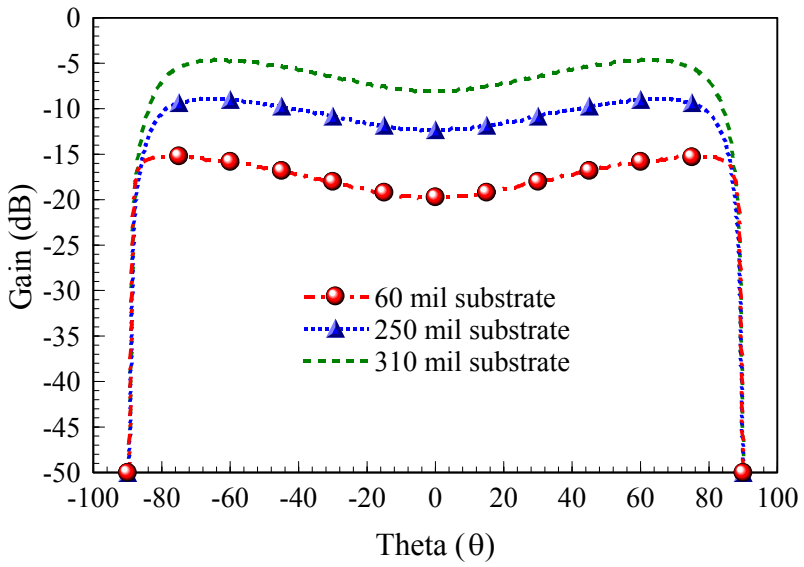

Figure 3.17: Plot of Simulated E-Plane Radiation Pattern for 3 Different Substrate Thicknesses for 1.3 GHz Meandered Shorted Patch Antenna

Expected E-Plane patterns for three substrate thicknesses of the Taconic substrate, (ε_r = 6.15), for the 2.6 GHz antenna are presented in Figures 3.18

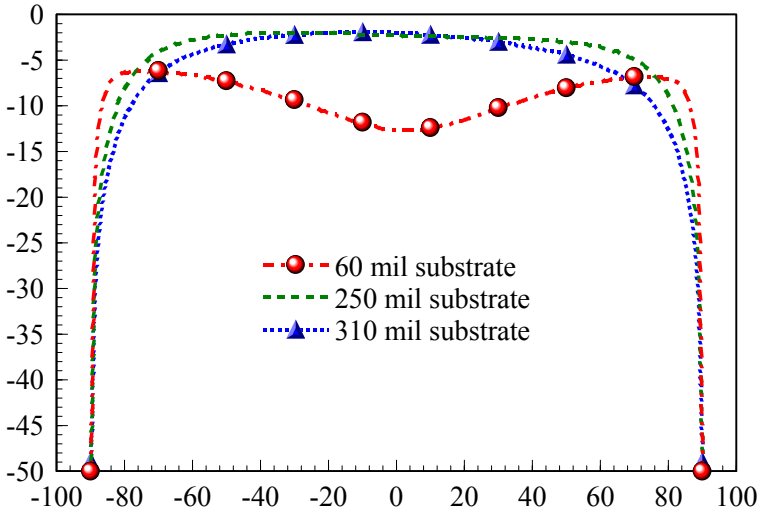

Figure 3.18: Plot of Simulated E-Plane Radiation Pattern Gain vs. Frequency for 3 Different Substrate Thicknesses for 1.3 GHz Meandered Shorted Patch Antenna

The data presented in Figures 3.17 and 3.18 indicate that the gain of the antennas increased as the substrate thickness increased. The thickness of the board was not further augmented to avoid bulkiness of the FDR.

Table 3.7 presents a comparison between the performance parameters of the quarter-wavelength shorted patch antennas employed in the first-generation FDR design and the meandered shorted patch antennas.

Table 3.7: Comparison of Simulated Parameters of Quarter-Wavelength Shorted Patch Antennas and Meandered Shorted Patch Antennas

Design	L / W (mm)	Gain (dB)	Efficiency (%)
1.3 GHz λ/4 Shorted Patch	22.5 / 17	-2.3	28.4
1.3 GHz Meandered Shorted Patch	9.54 / 5.05	-7.7	12.6
2.6 GHz λ/4 Shorted Patch	12.55 / 11	2.2	71.65
2.6 GHz Meandered Shorted Patch	7.25 / 3.25	-4.9	24.7

Table 3.8 illustrates the detrimental effect of reducing the size of the meandered shorted patch antennas on the parameters of gain and efficiency.

Table 3.8: Size Reduction between Quarter-Wavelength Shorted Patch Antennas and Meandered Shorted Patch Antennas

Frequency	Size Reduction (%)	Gain Reduction (%)	Efficiency Reduction (%)
1.3 GHz	87.4	70	55
2.6 GHz	82.9	55	65

The reduction in efficiency correlates very well with the discussion presented in Section 3.3. However, the increased substrate thickness played an important role in maintaining the efficiency and gain parameters of the meandered shorted patch antennas within acceptable limits, which compare to the antennas of the first-generation FDR design.

3.6.3 Radiation Patterns

Radiation pattern simulations and measured results were obtained using the same methodology described in Section 2.3.2. Antenna simulations were performed using ADS Momentum. The radiation pattern of the meandered shorted patch antennas was taken to be in the broadside direction (Refer to Figure 2.14, Chapter 2). The microstrip line feed was assumed to be parallel to the direction that the resonance occurred. Therefore, the radiation patterns were linearly polarized in the direction parallel to the microstrip feedline, which corresponded to $\Phi = 90^{\circ}$.

The antenna feedline was parallel to the E-Plane and perpendicular to the H-plane. As described in Section 2.3.2 for E-Plane simulated patterns, Φ was kept fixed at 90° and θ was swept 360°. H-plane simulated patterns maintained Φ fixed at 0° and θ was swept 360°. Electromagnetic simulations of the meandered shorted patch antennas were conducted utilizing a finite ground plane. The resulting radiation patterns again displayed considerable back-side radiation. The radiation patterns were normalized to the maximum co-polarization value obtained.

Figure 3.19 presents the co-polarized E and H-planes for the 1.3 GHz antenna at the particular frequency of interest. Figure 3.20 presents the co-polarized E and H-planes for the 2.6 GHz antenna at the particular frequency of interest. The plots indicate good agreement between the simulated and measured results.

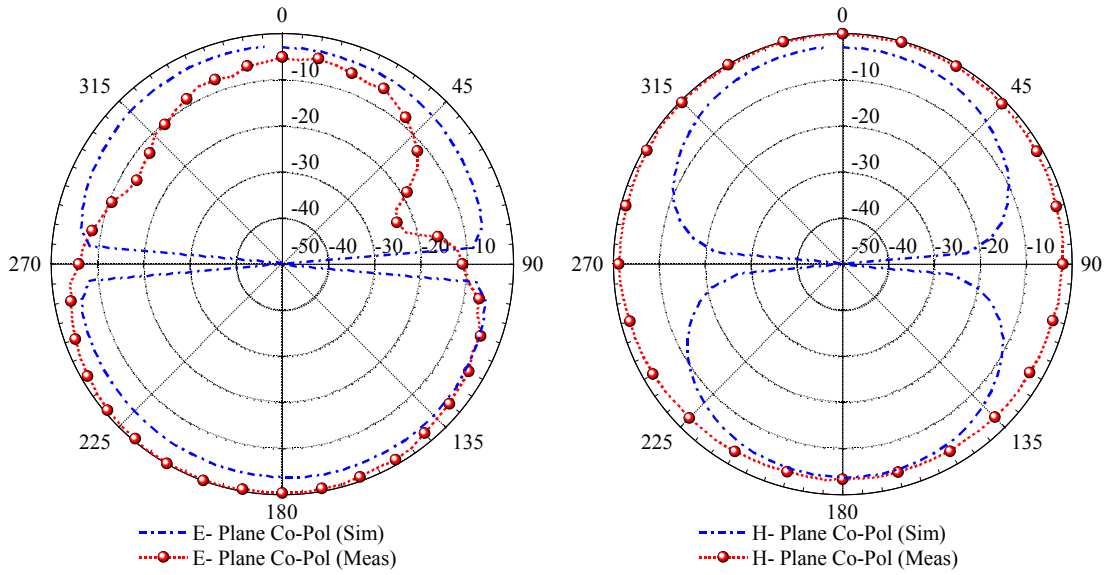

Figure 3.19: Comparison of Measured and Simulated Co-Polarized E-Plane (left) and H-Plane (right), Pattern of the 1.3 GHz Antenna, (dB)

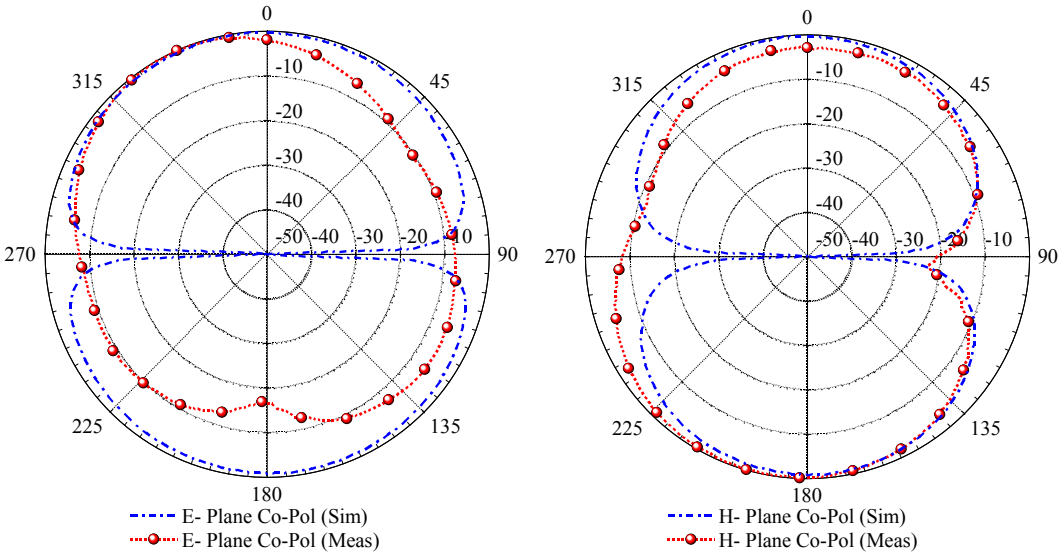

Figure 3.20: Comparison of Measured and Simulated Co-Polarized E-Plane (left) and H-Plane (right), Pattern of the 2.6 GHz Antenna, (dB)

E and H-plane cross-polarization measured patterns are presented in Figure 3.21.

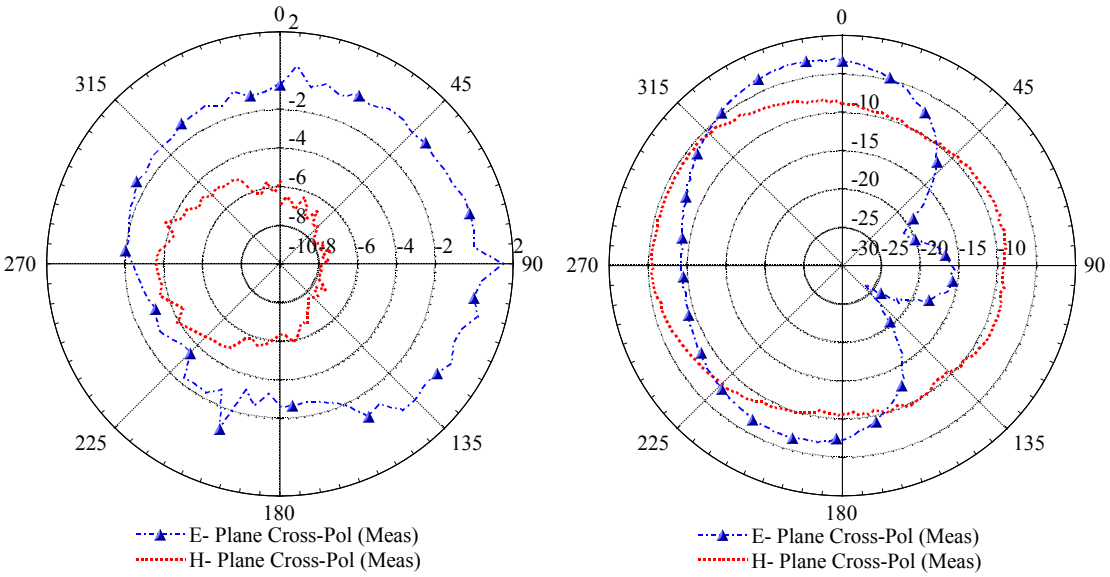

Figure 3.21: Cross-Polarized Measurement of the E and H-Plane Radiation Pattern of the 1.3 GHz Antenna (left) and 2.6 GHz Antenna (right), (dB)

The measurements were normalized to the maximum co-polarization value obtained for each antenna. Considerable cross-polarization is demonstrated. Some possible causes for the cross-polarization levels are also discussed in Section 2.3.2, of Chapter 2. A lowered width to length ratio of the antenna and the utilization of a microstrip feed can increase the polarization levels. Cross-polarization levels for shorted patch antennas have been reported to be higher than for half-wave patches, [2], [36]. Cross-polarization occurs since more current flows along the width of the quarter-wavelength antenna compared to a half-wavelength antenna since the width to length ratio is lower.

3.7 Conclusions

A review of antenna parameters, limitations of electrically small antennas and some of the techniques utilized in reducing the size of planar antennas has been

presented. A study of different meandered slot antenna design geometries for operation at 1.3 GHz was performed. It was shown from the meandered slot antenna designs presented that the reduction in size did not result in a significant reduction of the antenna's efficiency parameter. Effective meandering of the slot antenna geometry resulted in a minimal shift of the antenna's resonant frequency compared to the traditional CPW-fed slot antenna. Meandered shorted patch antennas operating at 1.3 GHz and 2.6 GHz were designed, fabricated, and measured. Good agreement occurred when comparing the expected and measured response for these electrically small antennas. The gain parameter for the meandered shorted patch antennas was improved by increasing the substrate thickness to 7.874 mm. The meandered shorted patch antennas studied yielded a reduction of approximately 85% in the overall size of the FDR design.

CHAPTER 4

A MINIATURIZED AND TUNABLE FREQUENCY DOUBLING REFLECTENNA

4.1 Introduction

The motivation for this research was a desire to design a compact frequency doubling reflectenna, which could be utilized primarily in sensing applications. The previous chapters of this thesis described the foundations for the realization of this miniature harmonic re-radiator. In Chapter 2, the methods used to design and to produce an efficient first-generation 1.3 GHz – 2.6 GHz FDR were presented. It was observed that in order to obtain a miniaturized FDR, the size of the input and output antennas had to be reduced. A discussion on electrically small antennas and the methodology utilized to achieve compact antennas, which were implemented in a second-generation FDR were outlined in Chapter 3.

This chapter presents a 1.3 GHz – 2.6 GHz miniature FDR design, which utilizes the meandered shorted patch antennas discussed in Chapter 3. Since the FDR operates at low input power levels, this research focused on producing an efficient device, which would exhibit low conversion loss values. Careful attention was focused, once more, on utilizing adequate performance prediction tools and measurement techniques. The miniature FDR obtained presented a size reduction of 74% and a maximum measured

conversion efficiency of 1.8%. The design of a compact tunable FDR will also be covered in this chapter. It was discovered that a re-configurable harmonic re-radiator can easily be obtained by employing variable impedance devices in its design.

4.2 Miniaturized 1.3 GHz - 2.6 GHz FDR Design

The design of the miniaturized frequency doubling reflectenna followed the same principles as presented for the first-generation design, which was discussed in Chapter 2. The FDR consisted of the receive and the transmit meandered shorted patch antennas, the diode doubler and matching circuits. As in the first-generation harmonic re-radiator, the HSCH-9161 GaAs Schottky diode was used as the doubling element.

Maximum power transfer was achieved when the doubler's circuit impedance was matched to the antenna's input impedance. The implementation of the meandered shorted patch antennas in the miniaturized FDR design resulted in a decrease of 8.8 dB of gain when compared to the quarter-wavelength shorted patch antennas used in the first-generation harmonic re-radiator. Therefore, maximum power transfer was especially important.

The meandered shorted patch antennas presented lower real input impedance and higher input reactance when compared to the quarter-wavelength shorted patch antennas used in the first-generation FDR. These parameter characteristics are natural for electrically small antennas. The antennas presented input impedances of

$$(12.7 + j335)\ \Omega \text{ at } 1.3 \text{ GHz}$$

and

$$(19.3 + j25.15)\ \Omega \text{ at } 2.6 \text{ GHz}.$$

The main objective of the FDR design was to achieve maximum conversion efficiency. Therefore, impedance matching circuits were designed to maximize the power transfer between the receive and transmit antennas and the input and output of the diode doubler. The input and output matching circuits consisted of distributed elements and surface mount components. Implementation of both types of elements ensured that low loss was achieved while compactness of the whole design was maintained.

The input matching circuit consisted of an open-circuited stub, a series 0.2 pF capacitor and a 100 nH shunt inductor. It was observed that the inclusion of a shunt inductor at input of the network improved the overall conversion efficiency of the design. At the output, the matching circuit consisted primarily of series distributed lines and a series 3.3 nH inductor. The overall circuit model for the miniaturized FDR design, which includes the impedance matching networks, is presented Figure 4.1.

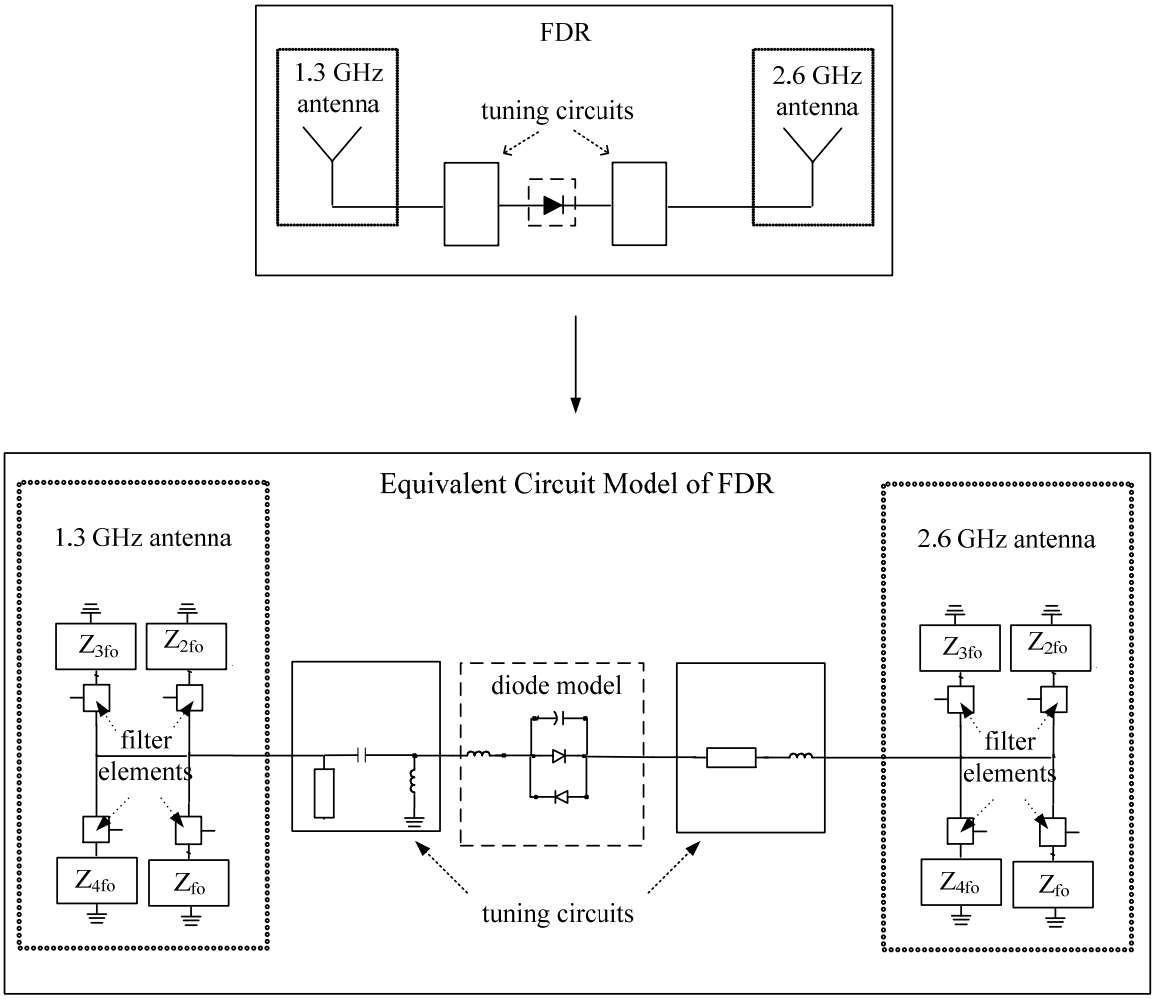

Figure 4.1: Overall Equivalent Circuit Model of Miniaturized Frequency Doubling Reflectenna for Computer-Aided Analysis

Agilent's Advanced Design System, (ADS), CAD software was utilized in order to predict the performance of this second-generation FDR. Conversion efficiency is given, as presented in Chapter2 by equation (2.1). Equation (2.1) is repeated here for convenience as equation (2.1):

$$\eta_n = \frac{P_{out}}{P_{in}}. \tag{2.1}$$

Chapter 2 presented a discussion on the criteria used to extract and determine the number of harmonics considered in the circuit simulations. Utilizing the results from that study, harmonic impedances up to the 4th order were utilized to predict the conversion loss of the diode doubler. It is important to note that this study was not done for the devices presented in this Chapter.

Figure 4.2 presents the conversion gain of the diode doubler for the miniaturized harmonic re-radiator.

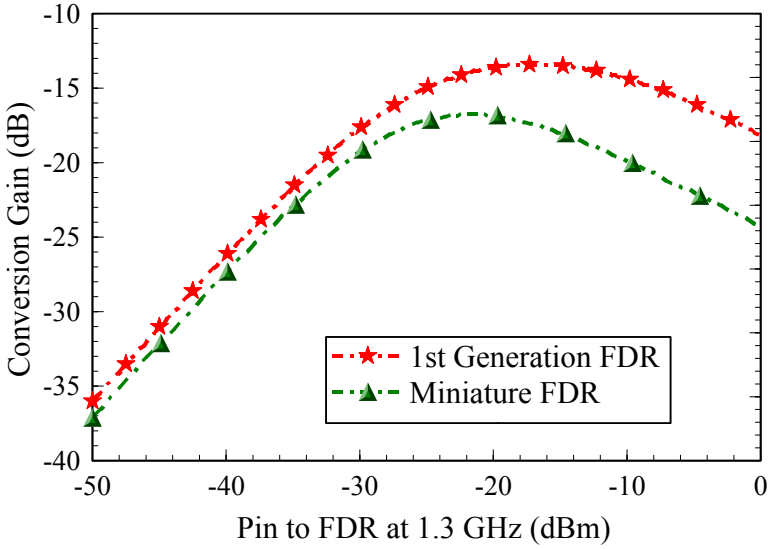

Figure 4.2: Simulated Conversion Gain for First-Generation FDR Diode Doubler and Miniaturized FDR Diode Doubler

The maximum predicted conversion gain was -16.7 dB at an input power to the diode doubler of -22.7 dBm. This maximum conversion gain was 3 dB lower than the first-generation FDR design. The decrease in conversion gain can be attributed to the loss, which occurs when impedance matching the high input reactance of the antennas to the impedance at the input and output of the diode doubler.

Figure 4.3 presents the design of a miniaturized FDR device.

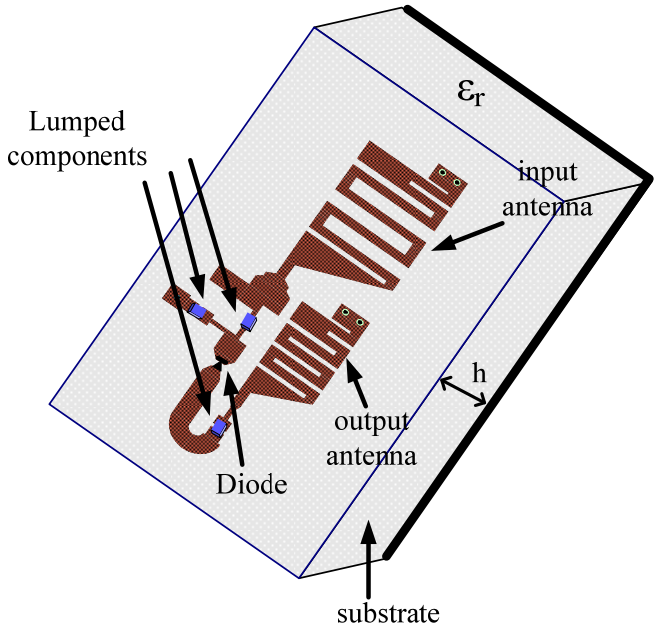

Figure 4.3: Illustration of Miniaturized Frequency Doubling Reflectenna

Substrate thickness was used to increase the gain of the meandered shorted patch antennas employed in the second-generation multiplier design. Therefore, the miniaturized FDR device was realized on a 310 mil thick Taconic substrate board with an ε_r of 6.15. The harmonic re-radiator measured 22 mm x 8.8 mm, which represents a size reduction of 75% in terms of length and width when compared to the first-generation FDR device.

4.3 Miniaturized and Tunable FDR Design

A final objective of the research presented in this thesis was to determine the feasibility of utilizing the FDR device for the RF transmission of modulated data. In order to demonstrate such a capability, a tunable harmonic re-radiator was designed. As

a sensor node, the FDR device would be encoding information by modulating the re-radiation. This information could then be decoded by a central transceiver system. Collection of data transmitted by the FDR sensor node was performed at the 2nd harmonic. The 2nd harmonic was used in order to alleviate the return that occurs from unwanted objects at the fundamental.

The tunable FDR was developed to operate either in an on-state or an off-state. In the on-state, the maximum achievable power transfer existed between the antennas and the diode doubler. Thus, the re-radiation at *2fo* was the maximum achievable. In an off-state, no re-radiation occurs at the 2nd harmonic.

In the on-state, maximum power transfer between the antennas and the diode doubler occurred when they were impedance matched. Therefore, maximum re-radiation occurred at the 2nd harmonic. In contrast, if the input impedance of the antennas is not well-matched to the source and load impedance of the diode, reduced re-radiation will occur. The FDR device would then be in an off-state.

During circuit simulations it was observed that the performance of the FDR device was most sensitive to effects at the input to the diode doubler. The impedance match between the receive antenna and the source terminal of the diode doubler can be modified by employing a variable reactance device, which modifies the impedance at the input of the network. Therefore, the variable reactance device could be operated in two states. One state would provide the reactance to ensure impedance match between the receive antenna and the input to the diode. A second state would impede maximum power transfer between the elements. This effect resulted in the harmonic re-radiator's desired on- and off-states.

In this research and as a proof-of-concept, a semiconductor varactor was chosen as the variable reactance device. The varactor employed was the Metelics MSV34,067-0805. A model of the Metelics varactor was developed by using S-parameter data and RF impedance data. Figure 4.4 diagrams the model of the varactor employed in computer-aided simulations.

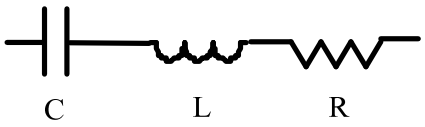

Figure 4.4: Circuit Model for the Metelics MSV34,067-0805 Varactor

In the model, *C* represents the series capacitance of the varactor, which can be described as the junction capacitance of a reversed biased junction as a function of the reverse bias voltage applied to the varactor. The junction capacitance, *C*, is given by

$$C(V) = \frac{C_{jo}}{(1 + \frac{V_r}{V_j})^m}. \tag{4.1}$$

In equation (4.1), three constants specify the junction capacitance. C_{jo} is the zero-bias junction capacitance, V_j is the junction potential and m is a unitless grading coefficient, which is a value that depends on the nature of the semiconductor junction of the varactor. V_r denotes the reverse bias potential applied to the varactor. The *L* parameter represents the series inductance and the *R* parameter represents the effective series resistance. The *L* and *R* parameters are the result of parasitic effects of the varactor component at RF

frequencies. The constants of the junction capacitance equation for the Metelics MSV34,067-0805 model, were found to be

$$C_{jo} = 2.05 \text{ pF},$$

$$V_j = 0.58 \text{ V}$$

$$m = 0.37.$$

The inductance value was found to be 1.74 nH.

The effective series resistance is given by

$$R = a + b \times freq^{0.5}, \tag{4.2}$$

where a and b are constants. For this particular varactor

$$a = 1.8,$$

$$b = 1.3 \text{ x } 10^{-5}.$$

The varactor was to be implemented at the input matching network. For ease in design, the varactor was implemented at the input matching network of the miniaturized FDR design. A 1.5 pF capacitor was placed in series with the varactor to obtain appropriate impedance for the shunt configuration that was comparable to the one obtained with the miniaturized harmonic re-radiator.

Bias was supplied to the varactor through a 10 KΩ resistor. The input matching circuit consisted of a shunt 1.5 pF capacitor, a 9.5 nH series inductor and a 8.2 nH shunt inductor. As in the miniaturized FDR design, at the output matching network, the matching circuit consisted primarily of series distributed lines and a series 3.3 nH inductor. Figure 4.5 presents the layout for the miniaturized FDR design, which includes the impedance matching networks and the varactor implementation.

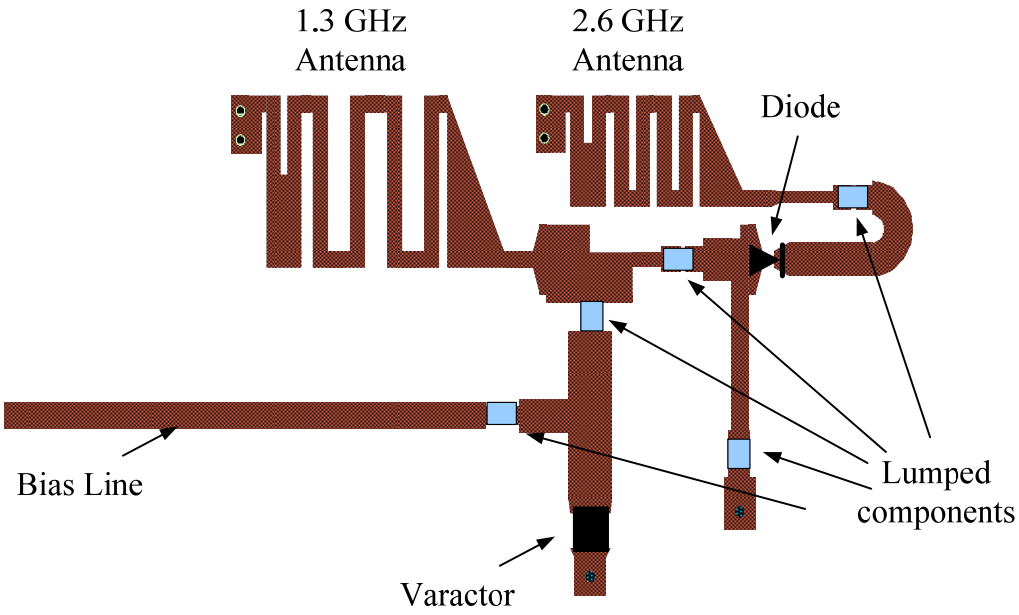

Figure 4.5: Layout of Tunable Frequency Doubling Reflectenna

Figure 4.6 presents the overall equivalent circuit model for the tunable FDR.

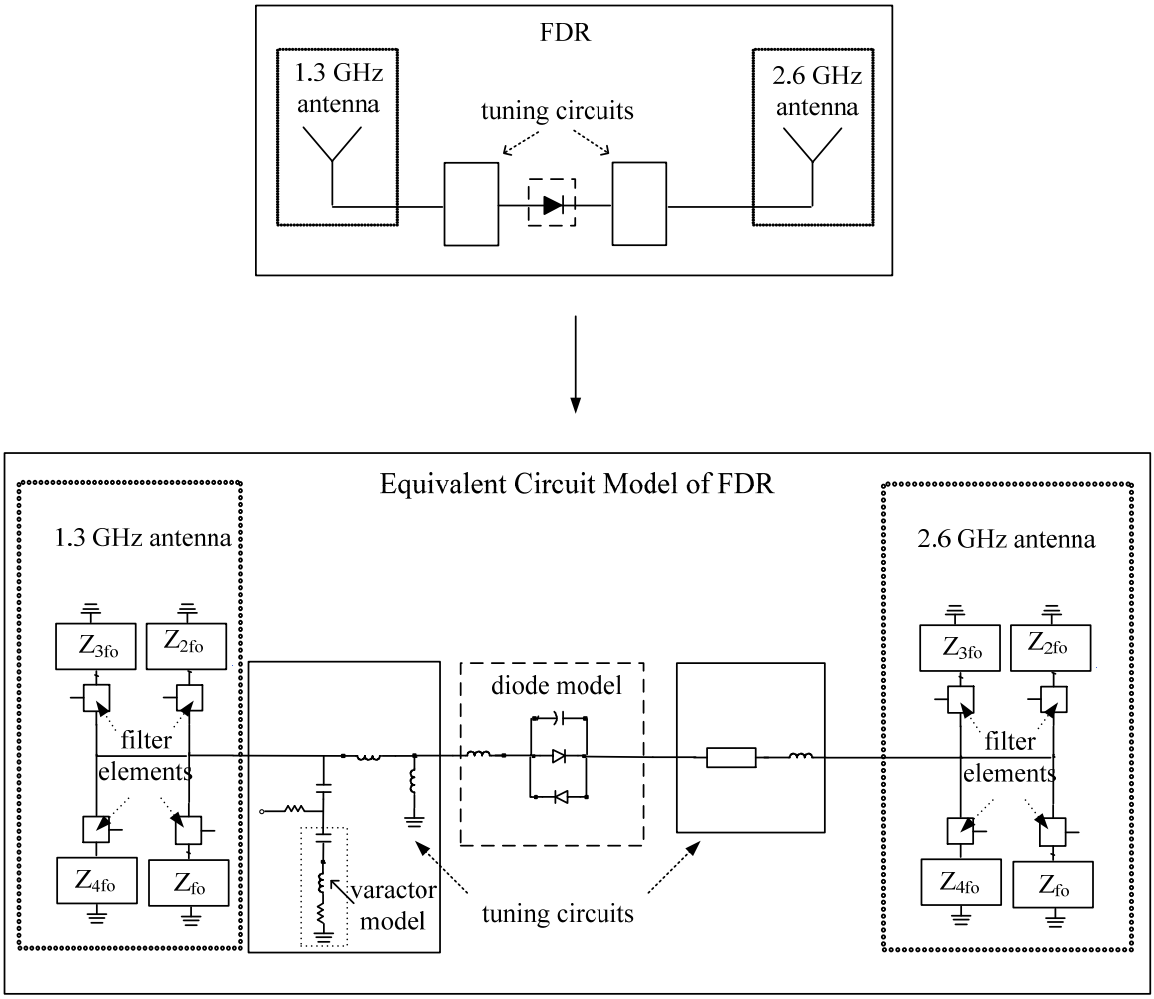

Figure 4.6: Overall Equivalent Circuit Model of Tunable Frequency Doubling Reflectenna for Computer-Aided Analysis

The varactor was operated at two different voltages. At a bias of 17 V, the varactor provided an impedance such that the conversion gain obtained from the diode doubler was optimum. When the varactor was biased with 0 V, the reactance it provided produced a significant change in the performance of the device. A significant difference in the conversion gain obtained from the diode doubler translated into a change in the frequency of operation of the device. Figure 4.7 illustrates this difference in conversion gain for the two different bias voltages.

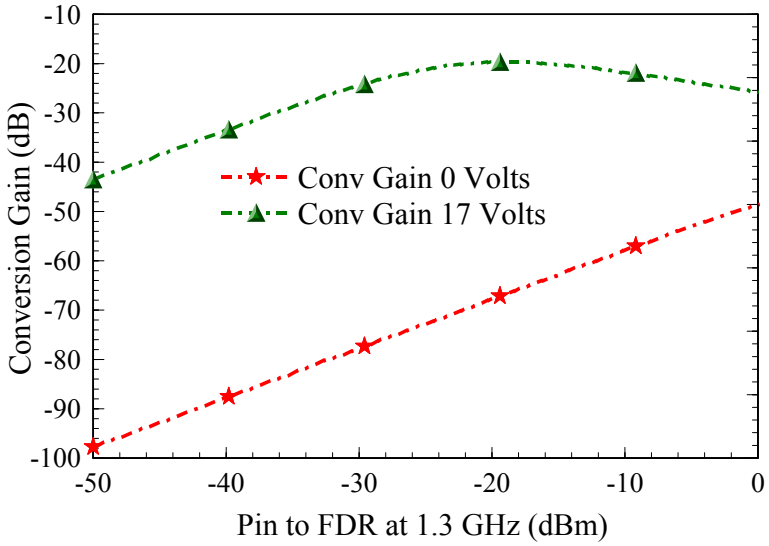

Figure 4.7: Simulated Conversion Gain for the Tunable FDR Diode Doubler: Maximum On Conversion Gain was Obtained when the Varactor was Biased at 17 V, (On-State)

Both the miniaturized and tuneable devices were fabricated and assembled in the same manner. The Taconic board with a substrate thickness of 310 mil and $\varepsilon_r = 6.15$, which was required for this design, was not readily available from the manufacturer. Therefore, a board with a thickness of 250 mil and one with a thickness 60 mil were bonded together using non-conductive epoxy. The copper on the substrate boards was patterned by using the standard copper etching techniques, which are described in Appendix A. The surface mount components were assembled on the board by using standard solder reflow techniques. Silver epoxy bonding was utilized to assemble the GaAs Schottky diode. The vias were soldered to ground using copper wires.

Figure 4.8 presents the conversion gain of the diode doubler for the three harmonic re-radiator designs.

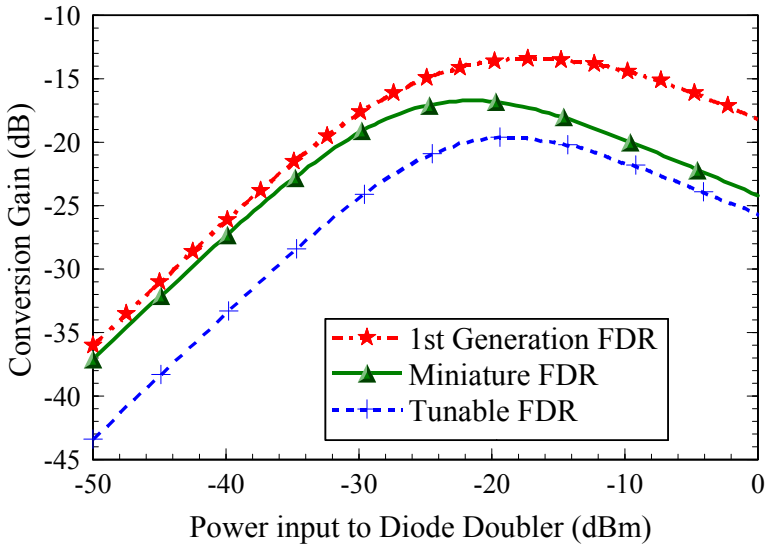

Figure 4.8: Simulated Conversion Gain for First-Generation FDR Diode Doubler, the Miniaturized FDR Diode Doubler and the Tunable FDR Diode Doubler when the Varactor was Biased at 17 V

The maximum predicted conversion gain for the tunable design was -19.6 dB at an input power to the diode doubler of -19.4 dBm. This maximum conversion gain was 6 dB lower than the first-generation FDR design. As described for the miniature design, the decrease in conversion gain can be attributed to the loss, which occurs when impedance matching the high input reactance of the antennas to the impedance at the input and output of the diode doubler. Also, the addition of a semiconductor varactor to the device increases loss due to a reduction of the quality factor of the network.

4.4 Results

Measurements on the miniature and tunable FDR devices, which were fabricated, were performed with the test measurement setup described in Section 2.4. The FDR was placed in an anechoic chamber, where it received the transmitted 1.3 GHz signal, doubled its frequency and reradiated it at 2.6 GHz. For an illustration of the hardware test-bench utilized for performing measurements refer to Section 2.4. Output power measurements were conducted using a spectrum analyzer, which was connected to the 2.6 GHz receiving antenna. There were two major differences to note from the first-generation measurement setup. A narrow bandpass filter was connected between the spectrum analyzer and the 2.6 GHz receiving antenna in order to filter out any unwanted harmonics. A high power amplifier with a power output of 40 dBm to provide input power levels to the diode doubler that were greater than -23.5 dBm was employed. The 22 dBm power output amplifier, described in Section 2.4, was used for input power levels to the multiplier, which were lower than -23.5 dBm. Path spreading losses were calculated using the free-space path loss formula.

The output power received at the 2.6 GHz antenna for two fabricated FDR devices was measured using the setup described above. The multiplier conversion gain values were calculated as well by using the relationship

$$CG = P_{out}(dB) - P_{in}(dB) + Receiving\ system\ loss(dB). \tag{4.3}$$

The output power received at the 2.6 GHz antenna is presented in Figure 4.9.

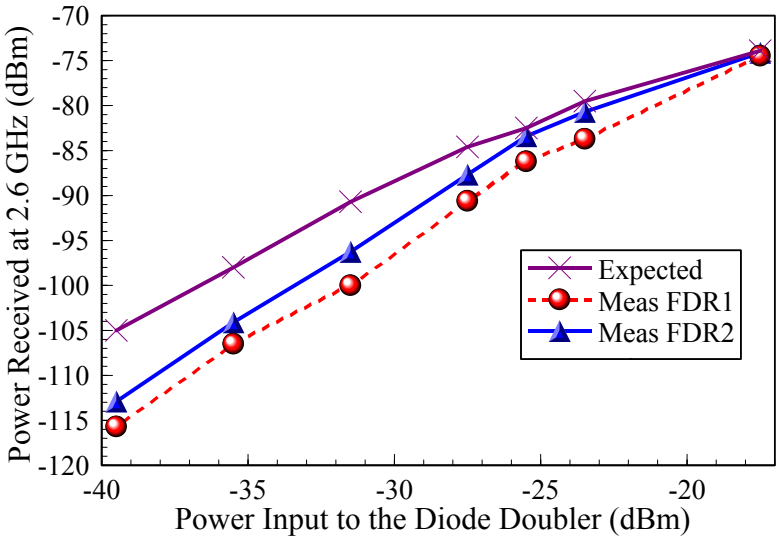

Figure 4.9: Comparison of Measured and Expected Doubler Power Received for the Miniaturized FDR at a Source Frequency of 1.3 GHz

The multiplier conversion loss curves for two miniature FDR's are presented in Figure 4.10.

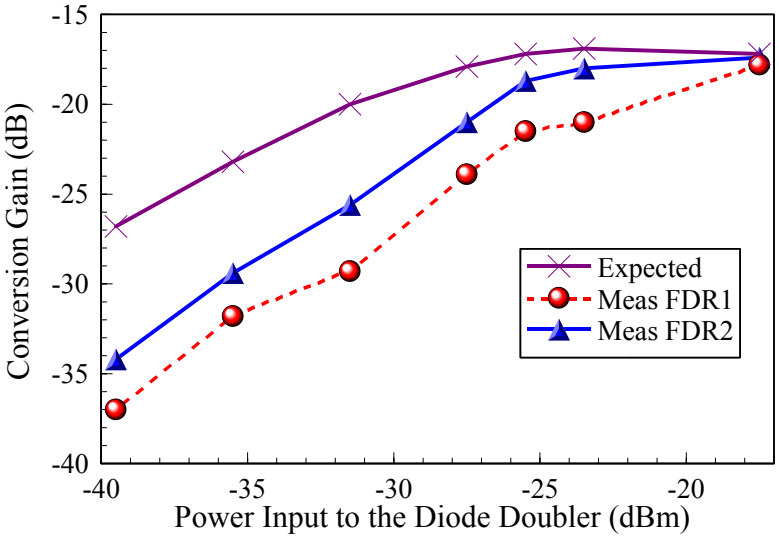

Figure 4.10: Comparison of Measured and Expected Doubler Conversion Gain for the Miniaturized FDR at a Source Frequency of 1.3 GHz

Good correlation can be observed between the measured curves for the miniature FDR's 1 and 2 and their expected performance. The measured conversion gain for miniature FDR 2 was -25.6 dB when the input power to the diode doubler was -31.5 dBm and a maximum value of -17.4 dB was obtained for an input power of -17.5 dBm. This translates into a maximum measured conversion efficiency of 1.8%. By considering the simulated value of gain of the input and output antennas, the measured conversion gain of the entire miniature FDR 2 was -33.5 dB for an input power level at the FDR receiving antenna of -23.5 dBm.

Measured values differed from simulated values as the input power level to the diode doubler decreased. The variation can be attributed to the fact that only up to fourth order harmonics were considered when performing circuit simulations. A study such as the one performed for the first-generation harmonic re-radiators, which observed the effect on the conversion loss values obtained when considering higher order harmonics was not conducted for these miniature devices. In addition, the frequency sensitivity of the miniature FDR's was not analyzed. The frequency at which the maximum doubler conversion efficiency occurred was not measured. The slight shift in performance might be due to fabrication tolerances.

The 1.3 GHz dual-patch array, which was used as the transmit antenna, possessed a narrowband response and provided less gain at frequencies other than at 1.3 GHz. If the multipliers perform optimally at a frequency not equal to 1.3 GHz, the gain used for calculations of the expected power received at 2.6 GHz might be an overestimation.

The measured output power received at the 2.6 GHz antenna for the tunable FDR is presented in Figure 4.11.

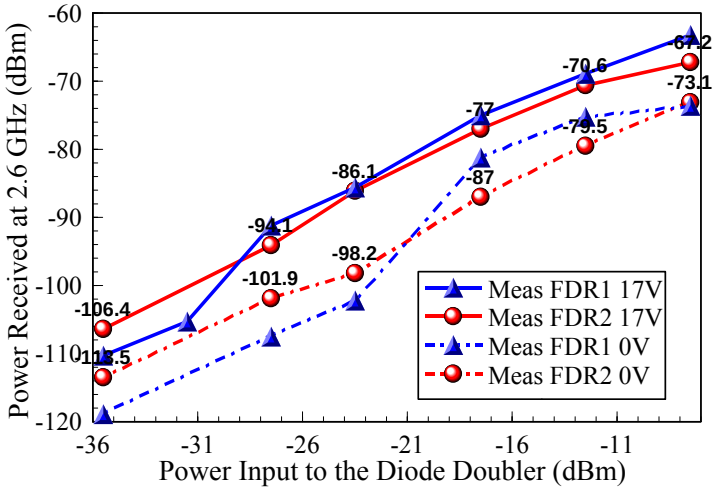

Figure 4.11: Comparison of Measured Doubler Power Received for the Tunable FDR at a Source Frequency of 1.3 GHz (Solid Lines Represent Performance of the Diode when Varactor was Biased at 17 V)

The multiplier conversion loss curves for the miniature tunable FDR are presented in Figure 4.12.

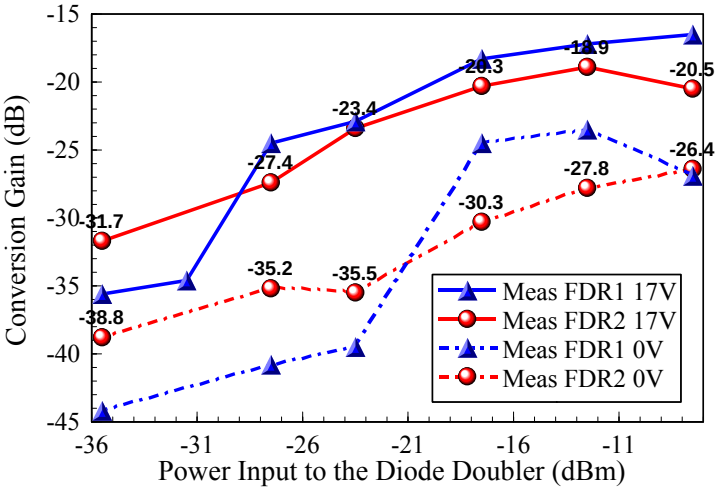

Figure 4.12: Comparison of Measured Doubler Conversion Gain for the Tunable FDR at a Source Frequency of 1.3 GHz (Solid Lines Represent Performance of the Diode when Varactor Biased at 17 V)

The measured results obtained from the tunable harmonic re-radiators fabricated illustrate the re-configurability of the device. In Figures 4.11 and 4.12, measured values are labeled for the tunable FDR 2 performance curves. As can be observed, the difference in bias voltage provided to the varactor caused a difference in conversion gain values in the range of 6 – 10 dB. This conversion gain variation demonstrates the tunability of the device.

The conversion gain for the tunable FDR 2 was -27.4 dB when the input power to the diode doubler was -27.5 dBm. A maximum value of -18.9 dB was obtained for an input power to the diode doubler of -12.2 dBm. These values translate to a maximum measured conversion efficiency of 1.3%. The conversion gain of the entire tunable harmonic re-radiator 2 was -35.4 dB for an input power level to the FDR receiving antenna of -19.5 dBm. This value was obtained by considering the simulated values for gain of the input and output antennas of the FDR device. These values correspond to optimum FDR operation which occurs when the varactor is biased at 17 V.

4.5 Conclusions

A miniaturized frequency doubling reflectenna was designed, fabricated and tested. At an input frequency of 1.3 GHz a multiplier conversion efficiency of 1.3% was obtained at an input power of -30 dBm. Meandered shorted patch antennas were successfully implemented in the design of the harmonic re-radiator. The harmonic re-radiators were produced using careful manufacturing methods and yielded a small spread in performance. It was demonstrated that the operation of the FDR device could be controlled by using a varactor element, which provided variable capacitance at the input

of the network. Due to the miniature and tunable designs achieved, the FDR exhibits great potential as a sensor node.

CHAPTER 5

SUMMARY AND RECOMMENDATIONS FOR FUTURE WORK

5.1 Summary

This thesis presented the research associated with the design of efficient and compact 1.3 GHz – 2.6 GHz frequency doubling reflectenna devices. The work focused on creating a simple and quasi-planar passive design, which would not require extremely precise manufacturing methods to produce. It was demonstrated that a miniature harmonic re-radiator, which operates efficiently at low input power levels, could be produced.

Significant attention was given to optimization of the conversion efficiency of the FDR. In order to optimize the conversion efficiency, the input impedances, at the frequencies of interest, of the receive and transmit antennas were approximately conjugate-matched to the input and output impedances of the diode doubler. Compact and low loss matching circuits were designed to maximize the power transfer between the antennas and the diode. The conversion gains of the harmonic re-radiators, described in this thesis, displayed an improvement over those reported for similar devices such as a Schottky diode doubler/antenna transponder design. A first-generation design yielded a conversion efficiency of 1% at a power input to the diode doubler of -30 dBm. Literature reports of comparable frequency multipliers coupled with antennas were operated at

higher input power levels, which provided for higher conversion efficiencies in those devices.

It was demonstrated that measurements obtained from both the first-generation and miniaturized FDR devices correlated well to the simulated values. In order to ensure accurate circuit simulations, the diode model parameters provided by the manufacturer were optimized. In addition, it was demonstrated that utilizing an adequate number of harmonic impedances, which were derived from the input and output antennas in the circuit simulations, provided for a more accurate prediction of the performance of the FDR.

The antennas utilized in the design of the harmonic re-radiators were shorted patch antennas. Implementation of quarter-wavelength shorted patch antennas produced a compact first-generation FDR device. These antenna designs were optimized for length and width to obtain desired input impedances at desired frequencies. This research focused on reducing the size of the first-generation harmonic re-radiator. A miniaturized FDR was developed as a second-generation device. Development of the second-generation device involved an in depth study of meandered shorted patch antennas. The meandered antenna provided the principle miniaturization mechanization for the second-generation device. In comparison with the quarter-wavelength shorted patch antennas utilized in the first-generation design, the electrically small meandered shorted patch antennas yielded a significant reduction in expected efficiency levels. It has been well-reported in the literature that antenna efficiency decreases as the volume that the antenna occupies decreases. It was demonstrated that by increasing the thickness of the substrate, used to implement the meandered shorted patch antennas, the expected values of antenna

efficiency and gain also increased. A study of the vias, which were used to short the patch antennas, revealed that via resistance must be minimized in order to obtain expected antenna efficiency and performance levels. It was observed that high levels of cross-polarization were exhibited by the shorted patch antennas used for the harmonic re-radiators. Therefore, shorted patch antennas can be utilized only if considerable levels of cross-polarization can be tolerated.

The first-generation FDR design measured 44 mm x 17 mm. The size of the miniaturized FDR device was reduced by 75%. The second-generation design resulted in a device that measured 22 mm x 8.8 mm. Due to the high input reactance values obtained from the meandered shorted patch antennas, which were utilized in the miniaturized design, losses associated with the matching networks of the miniaturized FDR device were higher. Therefore, the conversion efficiency, at an input power to the diode of -30 dBm, was 3 dB lower than the first-generation design.

A final accomplishment of this research was a demonstration of the tunability of the FDR device. It was demonstrated that the tunability of the FDR could be easily obtained by utilizing a variable reactance device at the input of the network. Therefore, the use of the frequency multiplier as a re-configurable device holds much potential.

5.2 Recommendations

Efficient passive multipliers, which can alleviate the clutter radiation that occurs at the frequency of the incident radiation in a radar transceiver system, are useful. The harmonic re-radiator described in this thesis is a promising device in sensing applications. The following are a few suggestions aimed at improving and extending this research.

In this research, a power input to the diode of -30 dBm was chosen as a benchmark value for design purposes. The impedance values of the diode, at the source and load, were dictated by this input power level. However, time-domain methods and harmonic balance simulations could be employed to provide a more in-depth analysis of the optimum power levels. Such an analysis would provide values for source and load impedances, which could maximize the conversion efficiency of the diode doubler. Then the input and output antennas of the network could be designed to be the conjugate-match of the optimum diode source and load impedances.

More consideration can be given to the compact antennas used for the harmonic re-radiator design. Even though the planar dimensions of the meandered shorted patch antenna designs decreased in size, substrate thickness was increased to optimize for efficiency and gain. In addition, the shorted patch antennas used in this design exhibited high levels of cross-polarization. Different types of electrically small antennas should be investigated to alleviate these shortcomings.

As an alternate choice, compact slot antennas could be utilized if the FDR design was to be implemented using a CPW layout configuration. Even if a CPW layout is not employed for the circuitry of the re-radiator, these antennas could still be used in conjunction with microstrip elements if a low loss and compact CPW-to-microstrip transition design was being considered. Slot antennas are less sensitive to manufacturing tolerances. Slot antennas can also be polarized in a desired manner using a combination of strip and slot conductors. In addition, a center-fed slot antenna can provide a high radiation resistance. The 1.3 GHz meandered slot antennas studied and described in this

thesis presented expected efficiency values, which were comparable to the first-generation quarter-wavelength shorted patch antennas.

A study of alternate multiplication elements could also be undertaken. Different diodes could be tested in order to select one that provided the best performance. Active devices such as FET's can also be employed to increase the conversion efficiency of the harmonic re-radiator if appropriate biasing schemes are investigated.

The research presented in this thesis can lead to the development of an FDR device, which can serve as a sensor for RF transmission of modulated data. The possibility of utilizing the FDR in a modulation scheme was not explored in this research. However, the design simplicity associated with obtaining a tunable FDR was demonstrated. As an extension of this research, analyzing alternate low loss integrated tuning structures, to replace the semiconductor varactor utilized in the present design, should be investigated.

Additional research associated with implementation of the FDR as a viable sensing device should be undertaken. The harmonic re-radiator could be tested in a multi-tone environment. Such testing would assess performance trends and levels when the device is subjected to several signals at different frequencies.

The data presented in this research were all broadside measurements. Measurements at different angles of incidence should be performed. A more detailed study of how the polarization levels affect the re-radiated signal from the FDR needs to be performed.

REFERENCES

[1] K. Chang, "Microwave Solid-State Circuits and Applications", John Wiley & Sons: New York, p.51, 1994

[2] R. Garg, P. Bhartia, I. Bahl and A. Ittipiboon, "Microstrip Antenna Design Handbook", Artech House: Norwood, MA, pp.1-657, 2001

[3] M. T. Faber, J. Chramiec and M. E. Adamski, "Microwave and Millimeter-Wave Diode Frequency Multipliers", Artech House: Norwood, MA, pp.1-87, 1995

[4] N. Paravastu, "Novel Frequency Multiplier Architectures for Millimeter Wave Applications." Ph.D. diss, University of Virginia, Charlottesville, VA, Jan. 2005

[5] E. Carman, K. Giboney, M. Case, M. Kamegawa, R. Yu, K. Abe and M.J.W. Rodwell, "28-39 GHz Distributed Harmonic Generation on a Soliton Nonlinear Transmission Line", IEEE Microwave and Guided Wave Letters, vol. 1, no. 2, pp.28-31, Feb. 1991

[6] E. Carman, M. Case, M. Kamegawa, R. Yu, K. Giboney and M.J.W. Rodwell, "V-band and W-band Broadband, Monolithic Distributed Frequency Multipliers", IEEE Intl. Microwave Symp. Digest, vol. 2, pp.819-822, June 1992

[7] S. Helbing, M. Cryan, F. Alimenti, P. Mezzanotte, L. Roselli and R. Sorrentino, "Design and Verification of a Novel Crossed Dipole Structure for Quasi-Optical Frequency Doublers", IEEE Microwave Guided Wave Letters, vol. 10, pp.105-107, Mar. 2000

[8] M. Kim, V. M. Lubecke, S. C. Martin, R. P. Smith and P. H. Siegel, "A Planar Parabola-Feed Frequency Multiplier", IEEE Microwave and Wireless Comp. Letters, vol. 7, pp.60-62, Mar. 1997

[9] S. B. Yeap, C. G. Parini, J. A. Dupuy and M. R. Rayner, "FDTD Simulation and Measurement of a 90 GHz Quasi-Optical Annular Slot Receiver", Proceedings, IEEE Microwaves, Antennas and Propagation, vol. 152, pp.117-123, Apr. 2005

[10] S. Hollung, J. Stake, L. Dillner and E. Kollberg, "A 141 GHz Integrated Quasi-Optical Slot Antenna Tripler", Proceedings, IEEE Microwaves, Antennas and Propagation Society, International Symposium, vol. 4, pp.2394-2397, Aug. 1999

[11] N. Paravastu and R.M. Weikle II, “A 40-80 GHz Quasi-Optical Balanced Doubler using Nested Ring-Slot Antennas”, IEEE Antennas and Propagation Society, International Symposium, vol.1, pp.270-273, 2002

[12] Y.H. Suh and K. Chang, “A High-Efficiency Dual-Frequency Rectenna for 2.45 and 5.8 GHz Wireless Power Transmission”, IEEE Transactions on Microwave Theory and Techniques, vol.50, no.7, pp.1784-1789, July 2002

[13] B.Strassner and K. Chang, “5.8 GHz Circularly Polarized Rectifying Antenna for Wireless Microwave Power Transmission”, IEEE Transactions on Microwave Theory and Techniques, vol.50, no.8, pp. 1870-1876, Aug. 2002

[14] T. Umeda, H. Yoshida, S. Sekine, Y. Fujita, T. Suzuki and S. Otaka, “A 950MHz Rectifier Circuit for Sensor Networks with 10m-distance”, IEEE International Solid-State Circuits Conference Digest, vol. 1, pp.256-597, Feb. 2005

[15] T. P. Ketterl, “Micro- and Nano-Scale Switches and Tuning Elements for Microwave Applications” Ph.D. diss, University of South Florida, Tampa, FL, Mar. 2006

[16] B.G. Colpitts and G. Boiteau, “Harmonic Radar Transceiver Design: Miniature Tags for Insect Tracking”, IEEE Transactions on Antennas and Propagation, vol.52, no.11, pp.2825-2832, Nov. 2004

[17] J. R. Riley and A. D. Smith, “Design Considerations for a Harmonic Radar to Investigate the Flight of Insects at Low Altitude”, Computers and Electronics in Agriculture, Elsevier, vol. 35, pp.151-169, Aug. 2002

[18] A. Polh, “A Review of Wireless SAW Sensors”, IEEE Transactions on Ultrasonics, Ferroelectrics and Frequency Control, vol.47, no.2, pp.317-332, Mar. 2000

[19] A. Pohl and F. Seifert, “New Applications of Wirelessly Interrogable Passive SAW Sensors”, IEEE Transactions on Microwave Theory and Techniques, vol.46, no.12, pp.2208-2212, Dec. 1998

[20] L.M. Reindl and I.M. Shrena, “Wireless Measurement of Temperature using Surface Acoustic Wave Sensors”, IEEE Transactions on Ultrasonics, Ferroelectrics and Frequency Control, vol.51, no.11, pp.1457-1463, Nov. 2004

[21] A.Pohl and F. Seifert, “Wirelessly Interrogable SAW-Sensors for Vehicular Applications”, Proceedings, IEEE Instrumentation and Measurement Technology Conference, Quality Measurements: The Indispensable Bridge between Theory and Reality, vol.2, June 1996, pp.1465-1468

[22] I.D. Robertson and I. Jaialy, “RF Id Tagging Explained”, Communications Engineer, vol.1, no.1, pp.20-23, Feb. 2003

[23] J. D. Griffin and G. D. Durgin, “Gains for RF Tags using Multiple Antennas”, IEEE Transactions on Antennas and Propagation, vol.56, no.2, pp.563-570, Feb. 2008

[24] F. Fuschini, C. Piersanti, F. Paolazzi and G. Falciasecca, “Analytical Approach to the Backscattering from UHF RFID Transponders”, IEEE Antennas and Wireless Propagation Letters, vol.7, pp.33-35, 2008

[25] Z. Fang, R. Jin and J. Geng, “Asymmetric Dipole Antenna Suitable for Active RFID Tags”, Electronics Letters, vol.44, no.2, pp.71-72, Jan. 2008

[26] W. Choi, H.W. Son, J. Yeo, J. Jae-young, J.H. Bae and C.G. Young, “Platform-Insensitive Antenna for RFID Sensor Tag in the UHF Band”, Proceedings, IEEE Antennas and Propagation Society, International Symposium, pp.2277-2280, June 2007

[27] M. Hirvonen, P. Pursula, K. Jaakkola and K. Laukkanen, “Planar Inverted-F Antenna for Radio Frequency Identification”, Electronics Letters, vol.40, no.14, pp.848-850, July 2004

[28] H.-E. Nilsson, J. Siden, T. Olsson, P. Jonsson and A. Koptioug, “Evaluation of a Printed Patch Antenna for Robust Microwave RFID Tags”, IEEE Transactions, Microwaves, Antennas & Propagation, vol.1, no.3, pp.776-781, June 2007

[29] M.J. DeVincentis, S. Ulker and R.M. Weikle II, “A Balanced HEMT Doubler for Quasi-Optical Applications”, IEEE Microwave and Guided Wave Letters, vol.9, no.6, pp.239-241, June 1999

[30] D. Singh, P. Gardner and P.S. Hall, “Integrated Push-Push Frequency Doubling Active Microstrip Transponder”, Electronics Letters, vol.33, no.6, pp.505-506, 13 Mar. 1997

[31] J. Birkeland and T. Itoh, “A Microstrip Based Active Antenna Doppler Transceiver Module”, 19th European Microwave Conference, pp.172-175, Oct. 1989

[32] C.W. Pobanz and T. Itoh, “A Microwave Non-Contact Identification Transponder using Sub-Harmonic Interrogation”, IEEE Transactions on Microwave Theory and Techniques, vol.43, no.7, pp.1673-1679, July 1995

[33] Y. Chung and T. Itoh, “A New Architecture for an AlGaN/GaN HEMT Frequency Doubler using an Active Integrated Antenna Design Approach”, Conference Proceedings Asia-Pacific Conference Proceedings, Nov. 2002

[34] T. Weller, “Activity Tag - Interim Report”, Univ. of South Florida, Tampa, FL, Raytheon Systems, Fullerton, CA, Interim Report, Feb. 2006

[35] J. Grajal, V. Krozer, E. González, F. Maldonado and J. Gismero, “Modeling and Design Aspects of Millimeter-Wave and Submillimeter-Wave Schottky Diode Varactor Frequency Multipliers”, IEEE Transactions on Microwave Theory and Techniques, vol. 48, pp. 700-711, Apr 2000

[36] G. Kumar and K.P. Ray, “Broadband Microstrip Antennas”, Artech House, Norwood, MA, pp. 1-248, 2003

[37] K.L. Wong, Compact and Broadband Microstrip Antennas, New York: John Wiley & Sons, 2002, pp.1-325

[38] D.M. Pozar, Microwave and RF Design of Wireless Systems, New York: John Wiley & Sons, 2001, pp.111-145

[39] C.A. Balanis, Antenna Theory, New York: John Wiley & Sons, 2nd ed., 1997, pp.28-570

[40] H.A. Wheeler, “Fundamental Limitations of Small Antennas,” Proceedings of the IRE, vol. 35, no. 12, Dec. 1947, pp.1479-1484

[41] L.J. Chu, “Physical Limitation of Omni-Directional Antennas,” Journal of Applied Physics, vol. 19, pp.1163-1175, Dec. 1948

[42] R.C. Hansen, "Fundamental limitations in antennas," Proceedings of the IEEE, vol.69, no.2, pp.170-182, Feb. 1981

[43] J. S. McLean, "A re-examination of the fundamental limits on the radiation Q of electrically small antennas," IEEE Transactions on Antennas and Propagation, vol.44, no.5, pp.672-676, May 1996

[44] H.A. Wheeler, "The Radiansphere around a Small Antenna," Proceedings of the IRE , vol.47, no.8, pp.1325-1331, Aug. 1959

[45] H. Wheeler, "Small antennas," IEEE Transactions on Antennas and Propagation, vol.23, no.4, pp.462-469, Jul 1975

[46] J.C.-E. Sten, A. Hujanen, P.K. Koivisto, "Quality factor of an electrically small antenna radiating close to a conducting plane," IEEE Transactions on Antennas and Propagation, vol.49, no.5, pp.829-837, May 2001

[47] A.D. Yaghjian, S.R. Best, "Impedance, bandwidth, and Q of antennas," IEEE Transactions on Antennas and Propagation, vol.53, no.4, pp.1298-1324, April 2005

[48] S.R. Best, "A discussion on the quality factor of impedance matched electrically small wire antennas," IEEE Transactions on Antennas and Propagation, vol.53, no.1, pp.502-508, Jan. 2005

[49] A.K. Skrivervik, J.-F. Zurcher, O. Staub, J.R. Mosig, "PCS antenna design: the challenge of miniaturization," IEEE Antennas and Propagation Magazine, vol.43, no.4, pp.12-27, Aug 2001

[50] K. L. Wong and S.C. Pan, "Compact triangular microstrip antenna," Electron Letters, vol 33, pp. 433-434, Mar. 1997

[51] D. Supriyo, R. Mittra, "Compact microstrip patch antenna," Microwave and Optical Technology Letters, vol. 13, no. 1, pp.12-14, 1996

[52] K. L. Lau, K.C. Kong, K. M. Luk, "A Miniature Folded Shorted Patch Antenna for Dual-Band Operation," IEEE Transactions on Antennas and Propagation, vol.55, no.8, pp.2391-2398, Aug. 2007

[53] T. Ozdernir, P. Frantzis, K.F. Sabet, L.P.B. Katehi, K. Sarabandi; J.F. Harvey, "Compact wireless antennas using a superstrate dielectric lens," IEEE Antennas and Propagation Society International Symposium, vol.3, no., pp.1678-1681, 2000

[54] H.Y. Wang, M.J. Lancaster, "Aperture-coupled thin-film superconducting meander antennas," IEEE Transactions on Antennas and Propagation, vol.47, no.5, pp.829-836, May 1999

[55] J. Lin; T. Itoh, "Active integrated antennas," IEEE Transactions on Microwave Theory and Techniques, vol.42, no.12, pp.2186-2194, Dec 1994

[56] V. A. Thomas; K.-M. Ling, M.E. Jones, B. Toland, J. Lin, T. Itoh, "FDTD analysis of an active antenna," IEEE Microwave and Guided Wave Letters, vol.4, no.9, pp.296-298, Sep 1994

[57] D.R. Jackson, N.G. Alexopoulos, "Simple approximate formulas for input resistance, bandwidth, and efficiency of a resonant rectangular patch," IEEE Transactions on Antennas and Propagation, vol.39, no.3, pp.407-410, Mar 1991

APPENDICES

Appendix A: Copper Etching Process Flow

The photoresist utilized in the process flow below is SC-1827 positive photoresist.

a. Clean the laminate board with acetone/methanol and nitrogen dry,
b. Dispense HMDS onto the board and spin at 3500 rpm for 30 seconds to dry completely,
c. Spin SC 1827 at 500 rpm for 15 seconds followed by 2000 rpm for 30 seconds,
d. Soft bake in the oven at 105˚C for 20 minutes, (lay the board flat),
e. Expose using broadband Quintel mask aligner for 55 seconds,
f. Immersion develop with slight agitation using MF 319 for ~75 seconds,
g. Clean with deionized, (DI), water and nitrogen dry,
h. Microscope inspect the image definition,
i. If protecting laminate backside, repeat steps b and c,
j. Hard bake in the oven at 110˚C for 20 minutes, (lay the board flat),
k. Ferric Chloride etch with slight agitation for ~8 minutes at 55˚C,
l. Clean with DI water and nitrogen dry,
m. Microscope inspect the image definition,
n. Remove photoresist with acetone/methanol.